

HOKKAIDO UNIVERSITY

Title	Hyper singular boundary element formulation for the Grad-Shafranov equation as an axisymmetric problem
Author(s)	Itagaki, Masafumi; Shimoda, Hiroshi
Citation	Engineering Analysis with Boundary Elements, 33(6), 845-857 https://doi.org/10.1016/j.enganabound.2008.11.003
Issue Date	2009-06
Doc URL	https://hdl.handle.net/2115/39402
Type	journal article
File Information	EABE33-6_p845-857.pdf



Hokkaido University Collection of Scholarly and Academic Papers : HUSCAP

Rev.

Hyper singular boundary element formulation for the Grad-Shafranov equation as an axisymmetric problem

Masafumi ITAGAKI, Hiroshi SHIMODA

Graduate School of Engineering, Hokkaido University,

Kita 13, Nishi 8, Kita-ku, Sapporo 060-8628, JAPAN

Tel. +81-11-706-6659

Fax. +81-11-706-7885

E-mail: itagaki@qe.eng.hokudai.ac.jp

This paper contains

31 pages of text,

4 tables and 13 figures.

Abstract

The Grad-Shafranov equation describes the magnetic flux distribution of plasma in an axisymmetric system such as a tokamak-type nuclear fusion device. This paper presents a scheme to solve the hyper singular boundary integral equation (HBIE) corresponding to this Grad-Shafranov equation. All hyper and strong singularities caused by differentials of the complete elliptic integrals have been regularized up to the level of the Cauchy principal value integral. Test calculations commonly using discontinuous boundary elements have been made to compare the HBIE solutions with the solutions of the standard boundary integral equation (SBIE).

Keywords: nuclear fusion, plasma, axisymmetric, Grad-Shafranov equation, complete elliptic integrals, hyper singular boundary integral equation, Cauchy principal value integral

1. Introduction

The magnetohydrodynamic (MHD) equilibrium of plasma in an axisymmetric (r, z) system such as a 'tokamak' nuclear fusion device is described by the Grad-Shafranov equation

$$-\left\{ r\frac{\partial}{\partial r}\left(\frac{1}{r}\frac{\partial}{\partial r}\right)+\frac{\partial^2}{\partial z^2}\right\}\psi = \mu_0 r j_\varphi \tag{1}$$

in terms of magnetic flux ψ and the toroidal component of of the plasma current j_φ **[1]**. The quantity μ_0 means the permeability in a vacuum. The boundary element method (BEM) **[2]** was applied to solving this equation **[3-5]**. In this application, the inhomogeneous current term $\mu_0 r j_\varphi$ is expanded into a 2-D polynomial

$$\mu_0 r\, j_\varphi \approx \sum_{l,m} \alpha_{l,m} r^l z^m . \qquad (l \geq 0,\ m \geq 0) . \tag{2}$$

The domain integral caused by $\mu_0 r j_\varphi$ is transformed into an equivalent boundary one, using a particular solution $\varphi^{(l,\,m)}$ corresponding to each term in the above polynomial **[3, 5]** and applying Green's second identity. The boundary integral equation for the plasma boundary Γ has the form

$$c_i\psi_i - \int_\Gamma \left(\frac{\psi^*}{r}\frac{\partial \psi}{\partial n} - \frac{\psi}{r}\frac{\partial \psi^*}{\partial n} \right) d\Gamma = \sum_{l,m} \alpha_{l,m} \left\{ c_i \varphi_i^{(l,m)} - \int_\Gamma \left(\frac{\psi^*}{r}\frac{\partial \varphi^{(l,m)}}{\partial n} - \frac{\varphi^{(l,m)}}{r}\frac{\partial \psi^*}{\partial n} \right) d\Gamma \right\}, \tag{3}$$

with the fundamental solution ψ^*. Itagaki et al. also applied the above boundary element formulation to an inverse analysis **[4]** where the plasma current density profile was reconstructed from signals of magnetic sensors located outside the plasma.

Apart from the above "standard" boundary integral equation (SBIE), the hyper singular boundary integral equation (HBIE) **[6-10]** arises when one takes a gradient of the SBIE. The authors have a future plan to introduce a HBIE approach into the above inverse analysis as an alternative to the SBIE or as a part of the combination of these two equations.

The HBIE corresponding to the Grad-Shafranov equation has never been solved before. As this

equation is for axisymmetric geometries, the fundamental solution and its derivatives are written mathematically in quite complicated forms all of which contain the complete elliptic integrals (see **Appendix**). Thus one needs to pay careful attention to their singularities when manipulating this type of HBIE.

In the present paper the HBIE for the Grad-Shafranov equation is regularized in a similar manner that Mansur et al. **[10]** used for the HBIE to solve the Laplace equation. A distinctive feature of the present work is that one must deal also with the polynomial expanded source. Even this inhomogeneous source generates a boundary integral, which also contains a hyper singular kernel.

Section 2 describes the process to transform the original HBIE into a form that is convenient to remove the singularities. The resultant boundary integral equation is given in **Section 2.5**. In **Section 3,** all boundary integral terms in the resultant equation are further rearranged in such a way that each term converges to a finite value. Discontinuous boundary elements are commonly used for all numerical examples given in **Section 4**, where the HBIE solutions are compared with the SBIE solutions.

2. Hyper singular boundary integral equation

One here starts with the standard boundary integral equation for an internal point i,

$$\psi_i - \int_\Gamma \left(\frac{\psi^*}{r}\frac{\partial \psi}{\partial n} - \frac{\psi}{r}\frac{\partial \psi^*}{\partial n} \right) d\Gamma = \sum_{l,m} \alpha_{l,m} \left\{ \varphi_i^{(l,m)} - \int_\Gamma \left(\frac{\psi^*}{r}\frac{\partial \varphi^{(l,m)}}{\partial n} - \frac{\varphi^{(l,m)}}{r}\frac{\partial \psi^*}{\partial n} \right) d\Gamma \right\}, \tag{4}$$

by substituting $c_i = 1.0$ into Eq.(3). The hyper singular boundary integral equation (HBIE) is given by differentiating Eq.(4) at the point i along an arbitrary direction $\mathbf{m} = (m_r, m_z)$. Using the notation $\partial / \partial m = \mathbf{m} \cdot \nabla$, the HBIE is written in the form

$$\frac{\partial \psi_i}{\partial m} - \int_\Gamma \left(\frac{1}{r}\frac{\partial \psi^*}{\partial m}\frac{\partial \psi}{\partial n} - \frac{\psi}{r}\frac{\partial^2 \psi^*}{\partial m \partial n} \right) d\Gamma = \sum_{l,m} \alpha_{l,m} \left\{ \frac{\partial \varphi_i^{(l,m)}}{\partial m} - \int_\Gamma \left(\frac{1}{r}\frac{\partial \psi^*}{\partial m}\frac{\partial \varphi^{(l,m)}}{\partial n} - \frac{\varphi^{(l,m)}}{r}\frac{\partial^2 \psi^*}{\partial m \partial n} \right) d\Gamma \right\}. \tag{5}$$

Consider a small semicircle of radius ε on the boundary as depicted in **Fig.1**. The source point i is assumed to be at the center of this semicircle and afterwards the radius ε is reduced to zero. In the following discussion, $\mathbf{x} = (r, z)$ denotes an arbitrary point along the boundary, while $\boldsymbol{\xi} = (a, b)$ means the source point i, i.e., the singular point.

Fig.1 Boundary surface augmented by a small semicircle of radius ε

Considering that the boundary is divided into Γ_ε and $\Gamma - \Gamma_\varepsilon$, Eq.(5) is rewritten in the form:

$$\begin{aligned}
&\frac{\partial \psi(\boldsymbol{\xi})}{\partial m} - \sum_{l,m} \alpha_{l,m} \frac{\partial \varphi^{(l,m)}(\boldsymbol{\xi})}{\partial m} \\
&- \int_{\Gamma - \Gamma_\varepsilon} \left(\frac{1}{r}\frac{\partial \psi^*}{\partial m}\frac{\partial \psi(\mathbf{x})}{\partial n} - \frac{\psi(\mathbf{x})}{r}\frac{\partial^2 \psi^*}{\partial m \partial n} \right) d\Gamma + \sum_{l,m} \alpha_{l,m} \int_{\Gamma - \Gamma_\varepsilon} \left(\frac{1}{r}\frac{\partial \psi^*}{\partial m}\frac{\partial \varphi^{(l,m)}(\mathbf{x})}{\partial n} - \frac{\varphi^{(l,m)}(\mathbf{x})}{r}\frac{\partial^2 \psi^*}{\partial m \partial n} \right) d\Gamma \\
&= \int_{\Gamma_\varepsilon} \left(\frac{1}{r}\frac{\partial \psi^*}{\partial m}\frac{\partial \psi(\mathbf{x})}{\partial n} - \frac{\psi(\mathbf{x})}{r}\frac{\partial^2 \psi^*}{\partial m \partial n} \right) d\Gamma - \sum_{l,m} \alpha_{l,m} \int_{\Gamma_\varepsilon} \left(\frac{1}{r}\frac{\partial \psi^*}{\partial m}\frac{\partial \varphi^{(l,m)}(\mathbf{x})}{\partial n} - \frac{\varphi^{(l,m)}(\mathbf{x})}{r}\frac{\partial^2 \psi^*}{\partial m \partial n} \right) d\Gamma.
\end{aligned} \tag{6}$$

2.1 Limiting forms of the fundamental solution and its derivatives

The fundamental solution ψ^* satisfies a subsidiary equation

$$-\Delta^* \psi^* = r\delta_i , \tag{7}$$

where δ_i means $\delta(r-a)\delta(z-b)$ with the spike at the point i having the coordinates (a,b). The mathematical form of ψ^* is given by **[3-5]**

$$\psi^* = \frac{\sqrt{ar}}{\pi k}\left[\left(1-\frac{k^2}{2}\right)K(k)-E(k)\right] \tag{8}$$

with

$$k^2 = \frac{4ar}{(r+a)^2+(z-b)^2}, \tag{9}$$

where $K(k)$ and $E(k)$ are the complete elliptic integrals of the first and second kinds, respectively. When the field point (r,z) approaches the source point (a,b), $K(k)$ and $E(k)$ can be approximated as **[11]**

$$K(k) \approx \frac{1}{2}\log\left(\frac{16}{1-k^2}\right) = \log\frac{1}{\varepsilon} + \log(4\sqrt{\varepsilon^2+4ar}) \tag{10a}$$

and

$$E(k) \approx 1, \tag{10b}$$

where $\varepsilon = \sqrt{(r-a)^2+(z-b)^2}$. Starting with Eqs.(10a) and (10b), the authors derived the limiting forms of the fundamental solution and its derivatives when $\varepsilon \to 0$ (The mathematical forms of the derivatives of ψ^* are listed in **Appendix**.). In this process, the relationships, $r-a = \varepsilon\cos\theta$ and $z-b = \varepsilon\sin\theta$ were used. The results are shown below.

First, the limit of the fundamental solution is given by

$$\psi^* \to \frac{a}{2\pi}\log\frac{1}{\varepsilon} + \frac{a}{2\pi}\log 8a - \frac{a}{\pi}. \tag{11}$$

Also, the derivatives of ψ^* with respect to a and b approach

$$\frac{\partial\psi^*}{\partial a} \to \frac{\log 8a - 1}{4\pi} - \frac{1}{4\pi}\cdot\log\varepsilon + \frac{a\cos\theta}{2\pi}\cdot\frac{1}{\varepsilon} \tag{12a}$$

and

$$\frac{\partial\psi^*}{\partial b} \to \frac{a\sin\theta}{2\pi}\cdot\frac{1}{\varepsilon} \tag{12b}$$

when $\varepsilon \to 0$, i.e., $r \to a$ and $z \to b$. As a linear combination of Eqs.(12a) and (12b), the

derivatives of ψ^* along the direction **m** takes the limit

$$\begin{aligned}
&\frac{\partial \psi^*}{\partial m} = m_r \frac{\partial \psi^*}{\partial a} + m_z \frac{\partial \psi^*}{\partial b} \\
&\to \frac{m_r(\log 8a - 1)}{4\pi} - \frac{m_r}{4\pi} \cdot \log \varepsilon + \frac{a(m_r \cos\theta + m_z \sin\theta)}{2\pi} \cdot \frac{1}{\varepsilon} \\
&\equiv D_0(\theta) + D_1(\theta) \log \varepsilon + D_2(\theta)/\varepsilon .
\end{aligned} \tag{13}$$

Next, one investigates the limit of $\partial^2 \psi / \partial m \partial n$. Based on the following four limits

$$\frac{\partial}{\partial a}\left(\frac{\partial \psi^*}{\partial r}\right) \to \frac{(2 - \log 8a) + \log 8a \cdot \cos 2\theta}{16\pi a} + \frac{1 - \cos 2\theta}{16\pi a} \cdot \log \varepsilon + \frac{\cos\theta}{2\pi} \cdot \frac{1}{\varepsilon} - \frac{a \cos 2\theta}{2\pi} \cdot \frac{1}{\varepsilon^2}, \tag{14a}$$

$$\frac{\partial}{\partial a}\left(\frac{\partial \psi^*}{\partial z}\right) \to \frac{(\log 8a + 1)\sin 2\theta}{16\pi a} - \frac{\sin 2\theta}{16\pi a} \cdot \log \varepsilon - \frac{\sin\theta}{4\pi} \cdot \frac{1}{\varepsilon} - \frac{a \sin 2\theta}{2\pi} \cdot \frac{1}{\varepsilon^2}, \tag{14b}$$

$$\frac{\partial}{\partial b}\left(\frac{\partial \psi^*}{\partial r}\right) \to \frac{(\log 8a - 1)\sin 2\theta}{16\pi a} - \frac{\sin 2\theta}{16\pi a} \cdot \log \varepsilon + \frac{\sin\theta}{4\pi} \cdot \frac{1}{\varepsilon} - \frac{a \sin 2\theta}{2\pi} \cdot \frac{1}{\varepsilon^2} \tag{14c}$$

and

$$\frac{\partial}{\partial b}\left(\frac{\partial \psi^*}{\partial z}\right) \to \frac{4 - \log 8a(3 + \cos 2\theta)}{16\pi a} + \frac{3 + \cos 2\theta}{16\pi a} \cdot \log \varepsilon + \frac{a \cos 2\theta}{2\pi} \cdot \frac{1}{\varepsilon^2}, \tag{14d}$$

one can write

$$\frac{\partial}{\partial m}\left(\frac{\partial \psi^*}{\partial n}\right) = \left(m_r \frac{\partial}{\partial a} + m_z \frac{\partial}{\partial b}\right)\left(n_r \frac{\partial}{\partial r} + n_z \frac{\partial}{\partial z}\right) \to C_0(\theta) + C_1(\theta) \log \varepsilon + \frac{C_2(\theta)}{\varepsilon} + \frac{C_3(\theta)}{\varepsilon^2} \tag{15}$$

with

$$\begin{aligned}
C_0(\theta) = \frac{1}{16\pi a}\big[&m_r n_r (2 - \log 8a) + m_z n_z (4 - 3\log 8a) + (m_r n_r - m_z n_z)\log 8a \cdot \cos 2\theta \\
&+ \{m_r n_z (1 + \log 8a) + m_z n_r (\log 8a - 1)\} \sin 2\theta \big],
\end{aligned} \tag{16a}$$

$$C_1(\theta) = \frac{1}{16\pi a}\{(m_r n_r + 3 m_z n_z) + (m_z n_z - m_r n_r)\cos 2\theta - (m_r n_z + m_z n_r)\sin 2\theta\}, \tag{16b}$$

$$C_2(\theta) = \frac{1}{4\pi}\{2 m_r n_r \cos\theta + (m_z n_r - m_r n_z)\sin\theta\} \tag{16c}$$

and

$$C_3(\theta) = \frac{a}{2\pi}\{(m_z n_z - m_r n_r)\cos 2\theta - (m_z n_r + m_r n_z)\sin 2\theta\}. \tag{16d}$$

That is, the limit of $\partial^2 \psi / \partial m \partial n$ given by Eq.(15) consists of the constant term, $\log \varepsilon$ (weak singularity), $1/\varepsilon$ (strong singularity) and $1/\varepsilon^2$ (hyper singularity).

2.2 Taylor series expansions of magnetic flux and its derivatives

One here assumes that the magnetic flux and its derivatives can be expanded in the form of a Taylor series expansion:

$$\psi(\mathbf{x}) = \psi(\xi) + (r-a)\frac{\partial\psi(\xi)}{\partial r} + (z-b)\frac{\partial\psi(\xi)}{\partial z} + \frac{\varepsilon^2}{2}[\cdots] + \cdots$$

$$= \psi(\xi) + \varepsilon\frac{\partial\psi(\xi)}{\partial n} + \frac{\varepsilon^2}{2}[\cdots] + \cdots, \tag{17}$$

$$\frac{\partial\psi(\mathbf{x})}{\partial r} = \frac{\partial\psi(\xi)}{\partial r} + \varepsilon\left[\cos\theta\frac{\partial^2\psi(\xi)}{\partial r^2} + \sin\theta\frac{\partial^2\psi(\xi)}{\partial r\partial z}\right] + \frac{\varepsilon^2}{2}[\cdots] + \cdots, \tag{18a}$$

$$\frac{\partial\psi(\mathbf{x})}{\partial z} = \frac{\partial\psi(\xi)}{\partial z} + \varepsilon\left[\cos\theta\frac{\partial^2\psi(\xi)}{\partial r\partial z} + \sin\theta\frac{\partial^2\psi(\xi)}{\partial z^2}\right] + \frac{\varepsilon^2}{2}[\cdots] + \cdots, \tag{18b}$$

and hence

$$\frac{\partial\psi(\mathbf{x})}{\partial n} = \frac{\partial\psi(\xi)}{\partial n}$$
$$+\varepsilon\left\{n_r\cos\theta\frac{\partial^2\psi(\xi)}{\partial r^2} + n_r\sin\theta\frac{\partial^2\psi(\xi)}{\partial r\partial z} + n_z\cos\theta\frac{\partial^2\psi(\xi)}{\partial r\partial z} + n_z\sin\theta\frac{\partial^2\psi(\xi)}{\partial z^2}\right\} + \frac{\varepsilon^2}{2}\{\cdots\} + \cdots, \tag{19}$$

where one used the relationship

$$\frac{\partial\psi(\mathbf{x})}{\partial n} = n_r\frac{\partial\psi(\mathbf{x})}{\partial r} + n_z\frac{\partial\psi(\mathbf{x})}{\partial z} \tag{20}$$

with $\mathbf{n} = (n_r, n_z)$.

First, one investigates the limit of the integral in Eq.(6)

$$\lim_{\varepsilon\to 0}\int_{\Gamma_\varepsilon}\frac{1}{r}\frac{\partial\psi^*}{\partial m}\frac{\partial\psi(\mathbf{x})}{\partial n}d\Gamma = \lim_{\varepsilon\to 0}\int_{\Gamma_\varepsilon}\frac{1}{r}\frac{\partial\psi^*}{\partial m}\left[\frac{\partial\psi(\xi)}{\partial n} + \varepsilon\{\cdots\} + \frac{\varepsilon^2}{2}\{\cdots\} + \cdots\right]\varepsilon d\theta,$$

where Eq.(19) and $d\Gamma = \varepsilon d\theta$ are introduced. As the singularity of $\partial\psi^*/\partial m$ can be given by Eq.(13), all terms multiplied by ε in Eq.(19) vanish. Then one finds

$$\boxed{\lim_{\varepsilon\to 0}\int_{\Gamma_\varepsilon}\frac{1}{r}\frac{\partial\psi^*}{\partial m}\frac{\partial\psi(\mathbf{x})}{\partial n}d\Gamma = \lim_{\varepsilon\to 0}\int_{\Gamma_\varepsilon}\frac{1}{r}\frac{\partial\psi^*}{\partial m}\frac{\partial\psi(\xi)}{\partial n}d\Gamma.} \tag{21}$$

Note here that the quantity $\partial\psi(\xi)/\partial n$ means

$$\frac{\partial\psi(\xi)}{\partial n} = n_r\frac{\partial\psi(\mathbf{x})}{\partial a} + n_z\frac{\partial\psi(\mathbf{x})}{\partial b} \quad . \tag{22}$$

Next, one investigates the limit of another integral

$$\lim_{\varepsilon\to 0}\int_{\Gamma_\varepsilon}\frac{\psi(\mathbf{x})}{r}\frac{\partial^2\psi^*}{\partial m\partial n}d\Gamma=\lim_{\varepsilon\to 0}\int_{\Gamma_\varepsilon}\frac{1}{r}\left[\psi(\xi)+\varepsilon\frac{\partial\psi(\xi)}{\partial n}+\frac{\varepsilon^2}{2}[\cdots]+\cdots\right]\frac{\partial^2\psi^*}{\partial m\partial n}\varepsilon d\theta\,.$$

Since the singularity of $\partial^2\psi^*/\partial m\partial n$ can be expressed by Eq.(15), the limit can be reduced to

$$\begin{aligned}\lim_{\varepsilon\to 0}\int_{\Gamma_\varepsilon}\frac{\psi(\mathbf{x})}{r}\frac{\partial^2\psi^*}{\partial m\partial n}d\Gamma&=\lim_{\varepsilon\to 0}\int_{\Gamma_\varepsilon}\frac{1}{r}\left[\psi(\xi)\left\{C_0(\theta)+C_1(\theta)\log\varepsilon+\frac{C_2(\theta)}{\varepsilon}+\frac{C_3(\theta)}{\varepsilon^2}\right\}\right]\varepsilon d\theta\\&\quad+\lim_{\varepsilon\to 0}\int_{\Gamma_\varepsilon}\frac{1}{r}\left[\varepsilon\frac{\partial\psi(\xi)}{\partial n}\left\{C_0(\theta)+C_1(\theta)\log\varepsilon+\frac{C_2(\theta)}{\varepsilon}+\frac{C_3(\theta)}{\varepsilon^2}\right\}\right]\varepsilon d\theta\\&=\lim_{\varepsilon\to 0}\int_{\Gamma_\varepsilon}\frac{1}{r}\left[\left\{C_2(\theta)+\frac{C_3(\theta)}{\varepsilon}\right\}\psi(\xi)\right]d\theta+\lim_{\varepsilon\to 0}\int_{\Gamma_\varepsilon}\frac{1}{r}\left[C_3(\theta)\frac{\partial\psi(\xi)}{\partial n}\right]d\theta.\end{aligned}\qquad(23)$$

If one finds

$$C_2(\theta)+\frac{C_3(\theta)}{\varepsilon}=\lim_{\varepsilon\to 0}\left(\varepsilon\frac{\partial^2\psi^*}{\partial m\partial n}\right),\ C_3(\theta)=\lim_{\varepsilon\to 0}\left(\varepsilon^2\frac{\partial^2\psi^*}{\partial m\partial n}\right)$$

and $\varepsilon d\theta=d\Gamma$, the relationship

$$\boxed{\lim_{\varepsilon\to 0}\int_{\Gamma_\varepsilon}\frac{\psi(\mathbf{x})}{r}\frac{\partial^2\psi^*}{\partial m\partial n}d\Gamma=\lim_{\varepsilon\to 0}\int_{\Gamma_\varepsilon}\frac{\psi(\xi)}{r}\frac{\partial^2\psi^*}{\partial m\partial n}d\Gamma+\lim_{\varepsilon\to 0}\int_{\Gamma_\varepsilon}\frac{\varepsilon}{r}\frac{\partial\psi(\xi)}{\partial n}\frac{\partial^2\psi^*}{\partial m\partial n}d\Gamma}\qquad(24)$$

can be obtained.

As the above two ideas can be applied again to the integrals for particular solutions, one also obtains

$$\boxed{\lim_{\varepsilon\to 0}\int_{\Gamma_\varepsilon}\frac{1}{r}\frac{\partial\psi^*}{\partial m}\frac{\partial\varphi^{(l,m)}(\mathbf{x})}{\partial n}d\Gamma=\lim_{\varepsilon\to 0}\int_{\Gamma_\varepsilon}\frac{1}{r}\frac{\partial\psi^*}{\partial m}\frac{\partial\varphi^{(l,m)}(\xi)}{\partial n}d\Gamma}\qquad(25)$$

and

$$\boxed{\lim_{\varepsilon\to 0}\int_{\Gamma_\varepsilon}\frac{\varphi^{(l,m)}(\mathbf{x})}{r}\frac{\partial^2\psi^*}{\partial m\partial n}d\Gamma=\lim_{\varepsilon\to 0}\int_{\Gamma_\varepsilon}\frac{\varphi^{(l,m)}(\xi)}{r}\frac{\partial^2\psi^*}{\partial m\partial n}d\Gamma+\lim_{\varepsilon\to 0}\int_{\Gamma_\varepsilon}\frac{\varepsilon}{r}\frac{\partial\varphi^{(l,m)}(\xi)}{\partial n}\frac{\partial^2\psi^*}{\partial m\partial n}d\Gamma.}\qquad(26)$$

Substituting Eqs.(21), (24), (25) and (26) into Eq.(6), one obtains

$$\begin{aligned}&\frac{\partial\psi(\xi)}{\partial m}-\sum_{l,m}\alpha_{l,m}\frac{\partial\varphi^{(l,m)}(\xi)}{\partial m}-\lim_{\varepsilon\to 0}\int_{\Gamma-\Gamma_\varepsilon}\left(\frac{1}{r}\frac{\partial\psi^*}{\partial m}\frac{\partial\psi(\mathbf{x})}{\partial n}-\frac{\psi(\mathbf{x})}{r}\frac{\partial^2\psi^*}{\partial m\partial n}\right)d\Gamma\\&+\sum_{l,m}\alpha_{l,m}\lim_{\varepsilon\to 0}\int_{\Gamma-\Gamma_\varepsilon}\left(\frac{1}{r}\frac{\partial\psi^*}{\partial m}\frac{\partial\varphi^{(l,m)}(\mathbf{x})}{\partial n}-\frac{\varphi^{(l,m)}(\mathbf{x})}{r}\frac{\partial^2\psi^*}{\partial m\partial n}\right)d\Gamma\end{aligned}$$

$$= \lim_{\varepsilon \to 0} \int_{\Gamma_\varepsilon} \left(\frac{1}{r} \frac{\partial \psi^*}{\partial m} \frac{\partial \psi(\xi)}{\partial n} - \frac{\psi(\xi)}{r} \frac{\partial^2 \psi^*}{\partial m \partial n} \right) d\Gamma - \lim_{\varepsilon \to 0} \int_{\Gamma_\varepsilon} \left(\frac{\varepsilon}{r} \frac{\partial \psi(\xi)}{\partial n} \frac{\partial^2 \psi^*}{\partial m \partial n} \right) d\Gamma$$

$$- \lim_{\varepsilon \to 0} \sum_{l,m} \alpha_{l,m} \int_{\Gamma_\varepsilon} \left(\frac{1}{r} \frac{\partial \psi^*}{\partial m} \frac{\partial \varphi^{(l,m)}(\xi)}{\partial n} - \frac{\varphi^{(l,m)}(\xi)}{r} \frac{\partial^2 \psi^*}{\partial m \partial n} \right) d\Gamma + \lim_{\varepsilon \to 0} \sum_{l,m} \alpha_{l,m} \int_{\Gamma_\varepsilon} \left(\frac{\varepsilon}{r} \frac{\partial \varphi^{(l,m)}(\xi)}{\partial n} \frac{\partial^2 \psi^*}{\partial m \partial n} \right) d\Gamma \tag{27}$$

2.3 Application of everywhere uniform magnetic flux

When one applies everywhere uniform magnetic flux ψ_0, both sides of the Grad-Shafranov equation (1) become zero. That is, there is no plasma current, in other words all polynomial expansion coefficient $\alpha_{l,m}$ must be zero. Equation (27) therefore becomes

$$\psi_0 \int_\Gamma \frac{1}{r} \frac{\partial^2 \psi^*}{\partial m \partial n} d\Gamma = \psi_0 \int_{\Gamma - \Gamma_\varepsilon} \frac{1}{r} \frac{\partial^2 \psi^*}{\partial m \partial n} d\Gamma + \psi_0 \int_{\Gamma_\varepsilon} \frac{1}{r} \frac{\partial^2 \psi^*}{\partial m \partial n} d\Gamma = 0 \tag{28a}$$

in this case. Also, if one assumes that the particular solution $\varphi = \sum_{l,m} \alpha_{l,m} \varphi^{(l,m)}$ is uniform, one finds

$$\left\{ \sum_{l,m} \alpha_{l,m} \varphi_0^{(l,m)} \right\} \left\{ \int_\Gamma \frac{1}{r} \frac{\partial^2 \psi^*}{\partial m \partial n} d\Gamma \right\}$$

$$= \left\{ \sum_{l,m} \alpha_{l,m} \varphi_0^{(l,m)} \right\} \left\{ \int_{\Gamma - \Gamma_\varepsilon} \frac{1}{r} \frac{\partial^2 \psi^*}{\partial m \partial n} d\Gamma \right\} + \left\{ \sum_{l,m} \alpha_{l,m} \varphi_0^{(l,m)} \right\} \left\{ \int_{\Gamma_\varepsilon} \frac{1}{r} \frac{\partial^2 \psi^*}{\partial m \partial n} d\Gamma \right\} = 0 . \tag{28b}$$

From both Eqs.(28a) and (28b), the relationship

$$\boxed{\int_{\Gamma_\varepsilon} \frac{1}{r} \frac{\partial^2 \psi^*}{\partial m \partial n} d\Gamma = - \int_{\Gamma - \Gamma_\varepsilon} \frac{1}{r} \frac{\partial^2 \psi^*}{\partial m \partial n} d\Gamma} \tag{29}$$

can be introduced. Using Eq.(29), Eq.(27) can be rearranged as

$$\frac{\partial \psi(\xi)}{\partial m} - \lim_{\varepsilon \to 0} \int_{\Gamma - \Gamma_\varepsilon} \left(\frac{1}{r} \frac{\partial \psi^*}{\partial m} \frac{\partial \psi(\mathbf{x})}{\partial n} - \frac{\psi(\mathbf{x}) - \psi(\xi)}{r} \frac{\partial^2 \psi^*}{\partial m \partial n} \right) d\Gamma$$

$$- \sum_{l,m} \alpha_{l,m} \frac{\partial \varphi^{(l,m)}(\xi)}{\partial m} + \lim_{\varepsilon \to 0} \sum_{l,m} \alpha_{l,m} \int_{\Gamma - \Gamma_\varepsilon} \left(\frac{1}{r} \frac{\partial \psi^*}{\partial m} \frac{\partial \varphi^{(l,m)}(\mathbf{x})}{\partial n} - \frac{\varphi^{(l,m)}(\mathbf{x}) - \varphi^{(l,m)}(\xi)}{r} \frac{\partial^2 \psi^*}{\partial m \partial n} \right) d\Gamma$$

$$= \lim_{\varepsilon \to 0} \int_{\Gamma_\varepsilon} \frac{1}{r} \frac{\partial \psi^*}{\partial m} \frac{\partial \psi(\xi)}{\partial n} d\Gamma - \lim_{\varepsilon \to 0} \int_{\Gamma_\varepsilon} \frac{\varepsilon}{r} \frac{\partial \psi(\xi)}{\partial n} \frac{\partial^2 \psi^*}{\partial m \partial n} d\Gamma$$

$$- \lim_{\varepsilon \to 0} \sum_{l,m} \alpha_{l,m} \int_{\Gamma_\varepsilon} \frac{1}{r} \frac{\partial \psi^*}{\partial m} \frac{\partial \varphi^{(l,m)}(\xi)}{\partial n} d\Gamma + \lim_{\varepsilon \to 0} \sum_{l,m} \alpha_{l,m} \int_{\Gamma_\varepsilon} \frac{\varepsilon}{r} \frac{\partial \varphi^{(l,m)}(\xi)}{\partial n} \frac{\partial^2 \psi^*}{\partial m \partial n} d\Gamma \tag{30}$$

2.4 Free term in hyper singular boundary integral equation

The first term on the RHS of Eq.(30) can be arranged in the forms

$$\begin{aligned}\lim_{\varepsilon\to 0}\int_{\Gamma_\varepsilon}\frac{1}{r}\frac{\partial\psi^*}{\partial m}\frac{\partial\psi(\xi)}{\partial n}d\Gamma &= \lim_{\varepsilon\to 0}\int_{\theta_1}^{\theta_2}\frac{1}{r}\left(D_0(\theta)+D_1(\theta)\log\varepsilon+D_2(\theta)/\varepsilon\right)\left(n_r\frac{\partial\psi}{\partial a}+n_z\frac{\partial\psi}{\partial b}\right)\varepsilon d\theta\\ &= \int_{\theta_1}^{\theta_2}\frac{1}{a}D_2(\theta)\left(n_r\frac{\partial\psi}{\partial a}+n_z\frac{\partial\psi}{\partial b}\right)d\theta\\ &= \int_{\theta_1}^{\theta_2}\frac{m_r\cos\theta+m_z\sin\theta}{2\pi}\left(\cos\theta\frac{\partial\psi}{\partial a}+\sin\theta\frac{\partial\psi}{\partial b}\right)d\theta\end{aligned} \tag{31}$$

by substituting Eq.(13), recalling $D_2(\theta)=a(m_r\cos\theta+m_z\sin\theta)/2\pi$ and considering that $n_r=\cos\theta$ and $n_z=\sin\theta$ along Γ_ε. Similarly, the second term on the RHS of Eq.(30) can be arranged as

$$\begin{aligned}&\lim_{\varepsilon\to 0}\int_{\Gamma_\varepsilon}\frac{\varepsilon}{r}\frac{\partial\psi(\xi)}{\partial n}\frac{\partial^2\psi^*}{\partial m\partial n}d\Gamma\\ &=\lim_{\varepsilon\to 0}\int_{\theta_1}^{\theta_2}\frac{\varepsilon}{r}\left(n_r\frac{\partial\psi}{\partial a}+n_z\frac{\partial\psi}{\partial b}\right)\left\{C_0(\theta)+C_1(\theta)\log\varepsilon+\frac{C_2(\theta)}{\varepsilon}+\frac{C_3(\theta)}{\varepsilon^2}\right\}\varepsilon d\theta\\ &=\int_{\theta_1}^{\theta_2}\frac{1}{a}\left(n_r\frac{\partial\psi}{\partial a}+n_z\frac{\partial\psi}{\partial b}\right)C_3(\theta)d\theta\\ &=\int_{\theta_1}^{\theta_2}\left(\cos\theta\frac{\partial\psi}{\partial a}+\sin\theta\frac{\partial\psi}{\partial b}\right)\frac{\{(m_z\sin\theta-m_r\cos\theta)\cos 2\theta-(m_z\cos\theta+m_r\sin\theta)\sin 2\theta\}}{2\pi}d\theta\\ &=-\int_{\theta_1}^{\theta_2}\left(\cos\theta\frac{\partial\psi}{\partial a}+\sin\theta\frac{\partial\psi}{\partial b}\right)\frac{(m_z\sin\theta+m_r\cos\theta)}{2\pi}d\theta\end{aligned} \tag{32}$$

by substituting Eq.(15) and recalling Eq.(16d). Except for the negative sign, Eq.(32) is identical to Eq.(31), i.e.,

$$\boxed{\lim_{\varepsilon\to 0}\int_{\Gamma_\varepsilon}\frac{1}{r}\frac{\partial\psi^*}{\partial m}\frac{\partial\psi(\xi)}{\partial n}d\Gamma=-\lim_{\varepsilon\to 0}\int_{\Gamma_\varepsilon}\frac{\varepsilon}{r}\frac{\partial\psi(\xi)}{\partial n}\frac{\partial^2\psi^*}{\partial m\partial n}d\Gamma.} \tag{33}$$

Equation (31) coupled with Eq. (32) can be further arranged as

$$
\begin{aligned}
&\lim_{\varepsilon\to 0}\int_{\Gamma_\varepsilon}\frac{1}{r}\frac{\partial\psi^*}{\partial m}\frac{\partial\psi(\boldsymbol{\xi})}{\partial n}d\Gamma-\lim_{\varepsilon\to 0}\int_{\Gamma_\varepsilon}\frac{\varepsilon}{r}\frac{\partial\psi(\boldsymbol{\xi})}{\partial n}\frac{\partial^2\psi^*}{\partial m\partial n}d\Gamma\\
&=\frac{1}{\pi}\int_{\theta_1}^{\theta_2}\left\{m_r\frac{\partial\psi}{\partial a}\cos^2\theta+(m_z\frac{\partial\psi}{\partial a}+m_r\frac{\partial\psi}{\partial b})\sin\theta\cos\theta+m_z\frac{\partial\psi}{\partial b}\sin^2\theta\right\}d\theta\\
&=\frac{\theta_2-\theta_1}{2\pi}\left(m_r\frac{\partial\psi}{\partial a}+m_z\frac{\partial\psi}{\partial b}\right)\\
&+\frac{\sin 2\theta_2-\sin 2\theta_1}{4\pi}\left(m_r\frac{\partial\psi}{\partial a}-m_z\frac{\partial\psi}{\partial b}\right)-\frac{\cos 2\theta_2-\cos 2\theta_1}{4\pi}(m_z\frac{\partial\psi}{\partial a}+m_r\frac{\partial\psi}{\partial b}).
\end{aligned}
\tag{34}
$$

When $\theta_2-\theta_1=\pi$, i.e., for a smooth boundary, one finds

$$
\boxed{
\begin{aligned}
&\lim_{\varepsilon\to 0}\int_{\Gamma_\varepsilon}\frac{1}{r}\frac{\partial\psi^*}{\partial m}\frac{\partial\psi(\boldsymbol{\xi})}{\partial n}d\Gamma-\lim_{\varepsilon\to 0}\int_{\Gamma_\varepsilon}\frac{\varepsilon}{r}\frac{\partial\psi(\boldsymbol{\xi})}{\partial n}\frac{\partial^2\psi^*}{\partial m\partial n}d\Gamma\\
&=\frac{1}{2}\left(m_r\frac{\partial\psi}{\partial a}+m_z\frac{\partial\psi}{\partial b}\right)=\frac{1}{2}\frac{\partial\psi(\boldsymbol{\xi})}{\partial m}.
\end{aligned}
}
\tag{35}
$$

The same manipulation can be applied to the integrals related to particular solutions on the RHS of Eq.(30), and when $\theta_2-\theta_1=\pi$, one obtains

$$
\boxed{
\begin{aligned}
&\lim_{\varepsilon\to 0}\int_{\Gamma_\varepsilon}\frac{1}{r}\frac{\partial\psi^*}{\partial m}\frac{\partial\varphi^{(l,m)}(\boldsymbol{\xi})}{\partial n}d\Gamma-\lim_{\varepsilon\to 0}\int_{\Gamma_\varepsilon}\frac{\varepsilon}{r}\frac{\partial\varphi^{(l,m)}(\boldsymbol{\xi})}{\partial n}\frac{\partial^2\psi^*}{\partial m\partial n}d\Gamma\\
&=\frac{1}{2}\left(m_r\frac{\partial\varphi^{(l,m)}}{\partial a}+m_z\frac{\partial\varphi^{(l,m)}}{\partial b}\right)=\frac{1}{2}\frac{\partial\varphi^{(l,m)}(\boldsymbol{\xi})}{\partial m}.
\end{aligned}
}
\tag{36}
$$

2.5 Resultant hyper singular boundary integral equation

Substituting Eqs.(35) and (36) into Eq.(30), one obtains

$$
\boxed{
\begin{aligned}
&\frac{1}{2}\frac{\partial\psi(\boldsymbol{\xi})}{\partial m}-\lim_{\varepsilon\to 0}\int_{\Gamma-\Gamma_\varepsilon}\left(\frac{1}{r}\frac{\partial\psi^*}{\partial m}\frac{\partial\psi(\mathbf{x})}{\partial n}-\frac{\psi(\mathbf{x})-\psi(\boldsymbol{\xi})}{r}\frac{\partial^2\psi^*}{\partial m\partial n}\right)d\Gamma\\
&=\sum_{l,m}\alpha_{l,m}\left\{\frac{1}{2}\frac{\partial\varphi^{(l,m)}(\boldsymbol{\xi})}{\partial m}-\lim_{\varepsilon\to 0}\int_{\Gamma-\Gamma_\varepsilon}\left(\frac{1}{r}\frac{\partial\psi^*}{\partial m}\frac{\partial\varphi^{(l,m)}(\mathbf{x})}{\partial n}-\frac{\varphi^{(l,m)}(\mathbf{x})-\varphi^{(l,m)}(\boldsymbol{\xi})}{r}\frac{\partial^2\psi^*}{\partial m\partial n}\right)d\Gamma\right\}
\end{aligned}
}
\tag{37}
$$

for a smooth boundary.

As the magnetic flux takes physically the same value along the plasma boundary, the term $\psi(\mathbf{x})-\psi(\boldsymbol{\xi})$ on the LHS of Eq.(37) must be zero regardless of the limitation. Because of this, Eq.(37) can be simplified as

$$\frac{1}{2}\frac{\partial\psi(\boldsymbol{\xi})}{\partial m}-\lim_{\varepsilon\to 0}\int_{\Gamma-\Gamma_\varepsilon}\frac{1}{r}\frac{\partial\psi^*}{\partial m}\frac{\partial\psi(\mathbf{x})}{\partial n}d\Gamma$$
$$=\sum_{l,m}\alpha_{l,m}\left\{\frac{1}{2}\frac{\partial\varphi^{(l,m)}(\boldsymbol{\xi})}{\partial m}-\lim_{\varepsilon\to 0}\int_{\Gamma-\Gamma_\varepsilon}\left(\frac{1}{r}\frac{\partial\psi^*}{\partial m}\frac{\partial\varphi^{(l,m)}(\mathbf{x})}{\partial n}-\frac{\varphi^{(l,m)}(\mathbf{x})-\varphi^{(l,m)}(\boldsymbol{\xi})}{r}\frac{\partial^2\psi^*}{\partial m\partial n}\right)d\Gamma\right\} \tag{38}$$

So far, the direction of m has been assumed to be arbitrary. If one defines m as the normal direction at the singular point $\boldsymbol{\xi}=(a,\,b)$ on a boundary, Eq.(38) can be discretized in the same procedure used for the standard boundary integral equation. The direction m is a fixed quantity, while n in Eq.(38) varies with the change in the integration point coordinates $\mathbf{x}=(r,\,z)$ along the boundary. Note that n agrees with m when $\mathbf{x}=(r,\,z)$ approaches $\boldsymbol{\xi}=(a,\,b)$.

2.6 Simple evaluation of the free term

It is interesting to point out that, if one assumes a special magnetic flux distribution, $\psi=r^2+z$, the LHS of the Grad-Shafranov equation (1) becomes zero. This means that both sides of the boundary integral equation, Eq.(37), must be zero when substituting $\psi=r^2+z$ (magnetic flux) or $\sum_{l,m}\alpha_{l,m}\varphi^{(l,m)}=r^2+z$ (particular solution). Then, in this case, one finds the condition

$$\frac{1}{2}\frac{\partial(r^2+z)}{\partial m}\bigg|_{\substack{r=a\\z=b}}-\lim_{\varepsilon\to 0}\int_{\Gamma-\Gamma_\varepsilon}\left(\frac{1}{r}\frac{\partial\psi^*}{\partial m}\frac{\partial(r^2+z)}{\partial n}-\frac{(r^2+z)-(a^2+b)}{r}\frac{\partial^2\psi^*}{\partial m\partial n}\right)d\Gamma=0. \tag{39}$$

That is, the validity of the present formulation and the accuracy of the numerical integration can be verified by checking if the condition

$$\lim_{\varepsilon\to 0}\int_{\Gamma-\Gamma_\varepsilon}\left\{\frac{1}{r}\frac{\partial\psi^*}{\partial m}\left(2r\cdot n_r+n_z\right)-\frac{(r^2+z)-(a^2+b)}{r}\frac{\partial^2\psi^*}{\partial m\partial n}\right\}d\Gamma\Big/\left(2a\cdot m_r+m_z\right)\equiv\frac{1}{2} \tag{40}$$

is satisfied or not.

3. Remarks on the singular integrals

3.1 Integrals in terms of $(1/r)(\partial^2\psi^*/\partial m\partial n)$

3.1.1 General outline

Now consider the boundary element Γ_O on which the singular point $\boldsymbol{\xi}=(a,b)$ exists. One here defines the distance between the singular point and an integration point $\mathbf{x}=(r,z)$ on Γ_O as

$$\rho=|\mathbf{x}-\boldsymbol{\xi}|=\sqrt{(r-a)^2+(z-b)^2}>0\,.$$

Using this distance, one rewrites the second integral on the RHS in Eq.(37) in the form

$$I=\int_{\Gamma_O-\Gamma_\varepsilon}\frac{\varphi^{(l,m)}(\mathbf{x})-\varphi^{(l,m)}(\boldsymbol{\xi})}{r}\frac{\partial^2\psi^*}{\partial m\partial n}d\Gamma=\int_{\Gamma_O-\Gamma_\varepsilon}\left(\frac{\varphi^{(l,m)}(\mathbf{x})-\varphi^{(l,m)}(\boldsymbol{\xi})}{\rho}\right)\left(\frac{\rho}{r}\frac{\partial^2\psi^*}{\partial m\partial n}\right)d\Gamma. \tag{41}$$

It should be noticed that the integral given by Eq.(41) is not defined at the singular point $\boldsymbol{\xi}=(a,b)$.

Dividing Eq.(41) into two parts at the point $\boldsymbol{\xi}$, one writes as

$$I=\int_{\Gamma_{-O}-\Gamma_\varepsilon}\left(\frac{\varphi^{(l,m)}(\mathbf{x})-\varphi^{(l,m)}(\boldsymbol{\xi})}{\rho}\right)\left(\frac{\rho}{r}\frac{\partial^2\psi^*}{\partial m\partial n}\right)d\Gamma+\int_{\Gamma_{+O}-\Gamma_\varepsilon}\left(\frac{\varphi^{(l,m)}(\mathbf{x})-\varphi^{(l,m)}(\boldsymbol{\xi})}{\rho}\right)\left(\frac{\rho}{r}\frac{\partial^2\psi^*}{\partial m\partial n}\right)d\Gamma. \tag{42}$$

Integration points $\mathbf{x}$ are located on the downstream side (Γ_{-O}) of Γ_o for the first term in Eq.(42), while $\mathbf{x}$ on the upstream side (Γ_{+O}) of Γ_o for the second term. That is, in the first integral the direction of $\mathbf{x}-\boldsymbol{\xi}$ is opposite to the direction of boundary integral $\boldsymbol{\Gamma}(\mathbf{x})$, while in the second integral both directions agree with each other. Then, when $\rho\to 0$ ($r\to a,\ z\to b$), the quantities $(\varphi^{(l,m)}(\mathbf{x})-\varphi^{(l,m)}(\boldsymbol{\xi}))/\rho$ in the first and the second integrals converges to different values of differential coefficient, as follows:

$$\lim_{\rho\to 0}\left(\frac{\varphi^{(l,m)}(\mathbf{x})-\varphi^{(l,m)}(\boldsymbol{\xi})}{\rho}\right)=\begin{cases}\left.\dfrac{\partial\varphi^{(l,m)}(\boldsymbol{\xi})}{\partial\Gamma}\right|_{\xi-} & (\lim_{\rho\to 0}(\mathbf{x}-\boldsymbol{\xi})\cdot\boldsymbol{\Gamma}(\mathbf{x})<0)\\ \left.\dfrac{\partial\varphi^{(l,m)}(\boldsymbol{\xi})}{\partial\Gamma}\right|_{\xi+} & (\lim_{\rho\to 0}(\mathbf{x}-\boldsymbol{\xi})\cdot\boldsymbol{\Gamma}(\mathbf{x})>0)\end{cases} \tag{43}$$

where one uses the subscripts $\xi-$ and $\xi+$ to mean the downstream and the upstream side from the singular point. Apparently, there is a relationship

$$\left.\frac{\partial\varphi^{(l,m)}(\boldsymbol{\xi})}{\partial\Gamma}\right|_{\xi-} = -\left.\frac{\partial\varphi^{(l,m)}(\boldsymbol{\xi})}{\partial\Gamma}\right|_{\xi+} \tag{44}$$

as long as the point $\boldsymbol{\xi}$ lies on a smooth boundary. From Eq.(15), one also knows

$$\lim_{\rho\to 0}\left(\frac{\rho}{r}\frac{\partial^2\psi^*}{\partial m\partial n}\right) = \lim_{\rho\to 0}\frac{1}{r}\left[C_2(\theta)+\frac{C_3(\theta)}{\rho}\right]. \tag{45}$$

The limit of the first term on the RHS of Eq.(45) is $C_2(\theta)/a$ and finite. The second term, where $C_3(\theta)$ is given by (16d), converges as

$$\lim_{\rho\to 0}\frac{1}{r}\frac{C_3(\theta)}{\rho} = \lim_{\rho\to 0}\frac{1}{2\pi\rho}\left\{(m_z n_z - m_r n_r)\cos 2\theta - (m_z n_r + m_r n_z)\sin 2\theta\right\} \to \frac{1}{2\pi\rho}, \tag{46}$$

since $m_r = n_r = \sin\theta$ and $m_z = n_z = -\cos\theta$ when $\rho \to 0$. One then obtains an approximation

$$\lim_{\rho\to 0}\left(\frac{\rho}{r}\frac{\partial^2\psi^*}{\partial m\partial n}\right) \approx \frac{1}{2\pi\rho} + const. \tag{47}$$

Considering Eqs.(43), (44) and (47), Eq.(41) can be rearranged in the form

$$\begin{aligned} I = &\int_{\Gamma_{-O}-\Gamma_\varepsilon}\left\{\frac{\varphi^{(l,m)}(\mathbf{x})-\varphi^{(l,m)}(\boldsymbol{\xi})}{r}\frac{\partial^2\psi^*}{\partial m\partial n} - \left.\frac{\partial\varphi^{(l,m)}(\boldsymbol{\xi})}{\partial\Gamma}\right|_{\xi-}\frac{1}{2\pi\rho}\right\}d\Gamma \\ &+\int_{\Gamma_{+O}-\Gamma_\varepsilon}\left\{\frac{\varphi^{(l,m)}(\mathbf{x})-\varphi^{(l,m)}(\boldsymbol{\xi})}{r}\frac{\partial^2\psi^*}{\partial m\partial n} - \left.\frac{\partial\varphi^{(l,m)}(\boldsymbol{\xi})}{\partial\Gamma}\right|_{\xi+}\frac{1}{2\pi\rho}\right\}d\Gamma \\ &+\frac{1}{2\pi}\left.\frac{\partial\varphi^{(l,m)}(\boldsymbol{\xi})}{\partial\Gamma}\right|_{\xi+}\left\{-\int_{\Gamma_{-O}-\Gamma_\varepsilon}\frac{1}{\rho}d\Gamma + \int_{\Gamma_{+O}-\Gamma_\varepsilon}\frac{1}{\rho}d\Gamma\right\}. \end{aligned} \tag{48}$$

The singularities at the first and the second terms on the RHS of Eq.(48) have been eliminated.

One here investigate the detail of the third term on the RHS of Eq.(48)

$$I_o = \frac{1}{2\pi}\left.\frac{\partial\varphi^{(l,m)}(\boldsymbol{\xi})}{\partial\Gamma}\right|_{\xi+}\left\{-\int_{\Gamma_{-O}-\Gamma_\varepsilon}\frac{1}{\rho}d\Gamma + \int_{\Gamma_{+O}-\Gamma_\varepsilon}\frac{1}{\rho}d\Gamma\right\}. \tag{49}$$

How the integral of Eq.(49) is made numerically?

3.1.2 Quadratic elements

First of all, one will consider the use of quadratic boundary element approximation **[12]**. Quadratic element expressions of the coordinates r and z along a boundary element are given by

$$r(\eta)=\frac{1}{2}\eta^2(r_- -2r_0+r_+)+\frac{1}{2}\eta(r_+ -r_-)+r_0 \tag{50a}$$

and

$$z(\eta)=\frac{1}{2}\eta^2(z_- -2z_0+z_+)+\frac{1}{2}\eta(z_+ -z_-)+z_0\,, \tag{50b}$$

using the dimensionless coordinate η $(-1\le\eta\le 1)$, the coordinates $(r_-,\, z_-)$, $(r_0,\, z_0)$ and $(r_+,\, z_+)$ at the mesh points shown in **Fig.2**. Similarly, using the dimensionless coordinate η_S corresponding to the singular point $\boldsymbol{\xi}(a,\, b)$, the coordinates a and b are given by

$$a=\frac{1}{2}\eta_S{}^2(r_- -2r_0+r_+)+\frac{1}{2}\eta_S(r_+ -r_-)+r_0 \tag{51a}$$

and

$$b=\frac{1}{2}\eta_S{}^2(z_- -2z_0+z_+)+\frac{1}{2}\eta_S(z_+ -z_-)+z_0\,. \tag{51b}$$

Fig.2 Quadratic boundary element

The distance between $\boldsymbol{\xi}(a,\, b)$ and $\mathbf{x}(r,\, z)$ can now expressed as

$$\begin{aligned}\rho&=\sqrt{\{r-a\}^2+\{z-b\}^2}\\&=\sqrt{\left\{\frac{\eta^2-\eta_S{}^2}{2}(r_- -2r_0+r_+)+\frac{\eta-\eta_S}{2}(r_+ -r_-)\right\}^2+\left\{\frac{\eta^2-\eta_S{}^2}{2}(z_- -2z_0+z_+)+\frac{\eta-\eta_S}{2}(z_+ -z_-)\right\}^2}\\&=|\eta-\eta_S|\sqrt{\left\{\frac{\eta+\eta_S}{2}(r_- -2r_0+r_+)+\frac{r_+ -r_-}{2}\right\}^2+\left\{\frac{\eta+\eta_S}{2}(z_- -2z_0+z_+)+\frac{z_+ -z_-}{2}\right\}^2}\,.\end{aligned} \tag{52}$$

On the other hand, the Jacobian $|J(\eta)|$ used in the following type of numerical integral,

$$\int_\Gamma f(\mathbf{r})d\Gamma=\int_{-1}^{1}f(\eta)|J(\eta)|d\eta,\quad i.e.,\ d\Gamma=|J(\eta)|\,d\eta\,, \tag{53}$$

has the form of

$$|J(\eta)|=\sqrt{\left(\frac{dr}{d\eta}\right)^2+\left(\frac{dz}{d\eta}\right)^2}=\sqrt{\left\{(r_- -2r_0+r_+)\eta+\frac{r_+ -r_-}{2}\right\}^2+\left\{(z_- -2z_0+z_+)\eta+\frac{z_+ -z_-}{2}\right\}^2}\,. \tag{54}$$

Equation (52) can be therefore expressed in the form

$$\rho = |\eta - \eta_S| \cdot \left| J\left(\frac{\eta + \eta_S}{2} \right) \right| \tag{55}$$

with the use of the Jacobian given by Eq.(54). Consequently, Eq.(49) can be rewritten as

$$I_o = \frac{1}{2\pi} \frac{\partial \varphi^{(l,m)}(\boldsymbol{\xi})}{\partial \Gamma}\bigg|_{\xi_+} \cdot \lim_{\delta \to 0} \left\{ \int_{-1}^{\eta_S - \delta} \frac{1}{\eta - \eta_S} \cdot \frac{|J(\eta)|}{\left| J\left(\frac{\eta + \eta_S}{2} \right) \right|} d\eta + \int_{\eta_S + \delta}^{1} \frac{1}{\eta - \eta_S} \cdot \frac{|J(\eta)|}{\left| J\left(\frac{\eta + \eta_S}{2} \right) \right|} d\eta \right\}. \tag{56}$$

Note that $|J\{(\eta + \eta_S)/2\}|$ and $|J(\eta)|$ in Eq.(56) agree to each other when $\eta = \eta_S$. Then, Eq.(56) can be further rearranged in the form

$$\begin{aligned} I_o = & \frac{1}{2\pi} \frac{\partial \varphi^{(l,m)}(\boldsymbol{\xi})}{\partial \Gamma}\bigg|_{\xi_+} \\ & \times \lim_{\delta \to 0} \left\{ \int_{-1}^{\eta_S - \delta} \left(\frac{1}{\eta - \eta_S} \cdot \frac{|J(\eta)|}{\left| J\left(\frac{\eta + \eta_S}{2} \right) \right|} - \frac{1}{\eta - \eta_S} \right) d\eta + \int_{\eta_S + \delta}^{1} \left(\frac{1}{\eta - \eta_S} \cdot \frac{|J(\eta)|}{\left| J\left(\frac{\eta + \eta_S}{2} \right) \right|} - \frac{1}{\eta - \eta_S} \right) d\eta \right\} \\ & + \frac{1}{2\pi} \frac{\partial \varphi^{(l,m)}(\boldsymbol{\xi})}{\partial \Gamma}\bigg|_{\xi_+} \cdot \lim_{\delta \to 0} \left\{ \int_{-1}^{\eta_S - \delta} \frac{1}{\eta - \eta_S} d\eta + \int_{\eta_S + \delta}^{1} \frac{1}{\eta - \eta_S} d\eta \right\}. \end{aligned} \tag{57}$$

The singularities in the first two integrals in Eq.(57) are eliminated, while the second term on the RHS is the Cauchy principal integral itself. Because of this, the quantity I_o can be numerically calculated as

$$I_o = \frac{1}{2\pi} \frac{\partial \varphi^{(l,m)}(\boldsymbol{\xi})}{\partial \Gamma}\bigg|_{\xi_+} \int_{-1}^{1} \left\{ \frac{1}{\eta - \eta_S} \cdot \frac{|J(\eta)|}{\left| J\left(\frac{\eta + \eta_S}{2} \right) \right|} - \frac{1}{\eta - \eta_S} \right\} d\eta + \frac{1}{2\pi} \frac{\partial \varphi^{(l,m)}(\boldsymbol{\xi})}{\partial \Gamma}\bigg|_{\xi_+} \cdot \log \left| \frac{1 - \eta_S}{1 + \eta_S} \right|. \tag{58}$$

The standard Gauss quadrature scheme **[13]** can be applied to the first term on the RHS of Eq.(58).

3.1.3 Straight line elements

The above discussion can be repeated for straight line boundary elements such as constant and linear elements when one assumes

$$r_0 = \frac{r_- + r_+}{2}, \quad z_0 = \frac{z_- + z_+}{2}. \tag{59}$$

Following Eq.(59), the coordinates (r, z) along a straight line elements can be written in the form

$$r(\eta) = \frac{1}{2}\eta(r_+ - r_-) + \frac{r_- + r_+}{2}, \quad z(\eta) = \frac{1}{2}\eta(z_+ - z_-) + \frac{z_- + z_+}{2}. \tag{60}$$

Also, the coordinates of the singular point (a, b) are given by

$$a = \frac{1}{2}\eta_S(r_+ - r_-) + \frac{r_- + r_+}{2}, \quad b = \frac{1}{2}\eta_S(z_+ - z_-) + \frac{z_- + z_+}{2}. \tag{61}$$

In this case, the distance ρ between the points (r, z) and (a, b) can be simply expressed as

$$\rho = |\eta - \eta_S| \sqrt{\left\{\frac{r_+ - r_-}{2}\right\}^2 + \left\{\frac{z_+ - z_-}{2}\right\}^2} \tag{62}$$

from Eq.(52). As the Jacobian is given by

$$|J(\eta)| = \sqrt{\left\{\frac{r_+ - r_-}{2}\right\}^2 + \left\{\frac{z_+ - z_-}{2}\right\}^2}. \tag{63}$$

in this case, one finds that Eq.(62) agrees with

$$\rho = |\eta - \eta_S| \cdot |J(\eta)|. \tag{64}$$

Since one can now write as (see Eq.(53))

$$\frac{d\Gamma}{\rho} = \frac{d\eta}{|\eta - \eta_S|}, \tag{65}$$

the integral I_o given by Eq.(49) is expressed in the form

$$\begin{aligned} I_o &= \frac{1}{2\pi}\frac{\partial\varphi^{(l,m)}(\boldsymbol{\xi})}{\partial\Gamma}\bigg|_{\xi+} \left\{ -\int_{\Gamma_- O - \Gamma_\varepsilon} \frac{1}{\rho} d\Gamma + \int_{\Gamma_+ O - \Gamma_\varepsilon} \frac{1}{\rho} d\Gamma \right\} \\ &= \frac{1}{2\pi}\frac{\partial\varphi^{(l,m)}(\boldsymbol{\xi})}{\partial\Gamma}\bigg|_{\xi+} \cdot \lim_{\delta\to 0}\left\{ \int_{-1}^{\eta_S - \delta} \frac{1}{\eta - \eta_S} d\eta + \int_{\eta_S + \delta}^{1} \frac{1}{\eta - \eta_S} d\eta \right\} \end{aligned} \tag{66}$$

for straight line boundary elements. As the RHS of Eq.(66) is described using the Cauchy principal value integral only, the value of I_o can be easily calculated as

$$I_0 = \frac{1}{2\pi}\frac{\partial\varphi^{(l,m)}(\boldsymbol{\xi})}{\partial\Gamma}\bigg|_{\xi+} \cdot \log\left|\frac{1-\eta_S}{1+\eta_S}\right| = \frac{1}{2\pi}\frac{\partial\varphi^{(l,m)}(\boldsymbol{\xi})}{\partial\Gamma}\bigg|_{\xi+} \cdot \log\frac{R_+}{R_-}. \tag{67}$$

Here, R_- and R_+ denote the values of distance ρ at two extreme points on a straight boundary

element. It should be noted that $I_o = 0$ for constant elements since $\eta_S = 0$ $(R_- = R_+)$ in this case.

3.2 Integrals in terms of $(1/r)(\partial\psi^*/\partial m)$

Next, one investigates the limits of the integrals

$$\lim_{\rho\to 0}\int_{\Gamma-\Gamma_\varepsilon}\frac{1}{r}\frac{\partial\psi^*}{\partial m}\frac{\partial\psi(\mathbf{x})}{\partial n}d\Gamma \quad \text{and} \quad \lim_{\rho\to 0}\int_{\Gamma-\Gamma_\varepsilon}\frac{1}{r}\frac{\partial\psi^*}{\partial m}\frac{\partial\varphi^{(l,m)}(\mathbf{x})}{\partial n}d\Gamma.$$

One already knows from Eq.(13) that, when $\rho\to 0$ $(r\to a,\ z\to b)$,

$$\begin{aligned}\frac{\partial\psi^*}{\partial m} &\to D_0(\theta)+D_1(\theta)\log\rho+D_2(\theta)/\rho \\ &= \frac{m_r(\log 8a-1)}{4\pi}-\frac{m_r}{4\pi}\cdot\log\rho+\frac{a}{2\pi}\cdot\frac{m_r\cos\theta+m_z\sin\theta}{\rho}.\end{aligned} \tag{68}$$

Now consider the term $(m_r\cos\theta+m_z\sin\theta)/\rho$ in Eq.(68). When $\rho\to 0$, the components of a unit normal vector, n_r and n_z, defined for any point on the boundary agree with those of m_r and m_z at the fixed point $\xi=(a,b)$, i.e., $n_r=\sin\theta\to m_r$ and $n_z=-\cos\theta\to m_z$. Because of this, $m_r\cos\theta+m_z\sin\theta$ approaches $-m_rm_z+m_zm_r=0$ in the limit. For straight-line boundary elements such as constant and linear elements, the term $(m_r\cos\theta+m_z\sin\theta)/\rho$ is entirely zero since $n_r=m_r$ and $n_z=m_z$ are satisfied independently of the limit $\rho\to 0$.

With the notations $\rho_r=r-a=\rho\cos\theta$ and $\rho_z=z-b=\rho\sin\theta$, the limit can be written as

$$\lim_{\rho\to 0}\frac{m_r\cos\theta+m_z\sin\theta}{\rho}=\lim_{\substack{\rho_r\to 0\\ \rho_z\to 0}}\frac{m_r\rho_r+m_z\rho_z}{\rho_r^2+\rho_z^2}. \tag{69}$$

As a matter of fact, this limit is finite even for quadratic and higher order boundary elements. The proof was already given at Section 4.2 in the previous work for SBIE **[5]**.

Equation (68) can now be expressed as

$$\frac{\partial\psi^*}{\partial m}\approx\frac{m_r}{4\pi}\log\frac{1}{\rho}+const. \tag{70}$$

when $\rho\to 0$, i.e., the points (a,b) and (r,z) approach each other. As a result, the boundary integrals in terms of $(1/r)(\partial\psi^*/\partial m)$ can be numerically performed as

$$\int_{\Gamma_o} \frac{1}{r}\frac{\partial \psi^*}{\partial m} d\Gamma = \int_{\Gamma_o} \left(\frac{1}{r}\frac{\partial \psi^*}{\partial m} - \frac{m_r}{4\pi a}\log\frac{1}{\rho} \right) d\Gamma + \int_{\Gamma_o} \frac{m_r}{4\pi a}\log\frac{1}{\rho} d\Gamma \tag{71a}$$

and

$$\begin{aligned} &\int_{\Gamma_o} \frac{1}{r}\frac{\partial \psi^*}{\partial m}\frac{\partial \varphi^{(l,m)}(\mathbf{x})}{\partial n} d\Gamma \\ &= \int_{\Gamma_o} \left(\frac{1}{r}\frac{\partial \psi^*}{\partial m}\frac{\partial \varphi^{(l,m)}(\mathbf{x})}{\partial n} - \frac{m_r}{4\pi a}\log\frac{1}{\rho}\cdot\frac{\partial \varphi^{(l,m)}(\boldsymbol{\xi})}{\partial n} \right) d\Gamma + \int_{\Gamma_o} \frac{m_r}{4\pi a}\log\frac{1}{\rho}\cdot\frac{\partial \varphi^{(l,m)}(\boldsymbol{\xi})}{\partial n} d\Gamma \end{aligned} \tag{71b}$$

when the point (a,b) is located within the boundary element under consideration. In each equation, the ordinary Gaussian quadrature rule can be applied to the first integral of the RHS, since the singularity is eliminated by the subtraction. The second integral can be performed analytically for constant and linear elements **[2]**, or can be dealt with accurately using the logarithmic Gaussian quadrature formula **[13]**.

4. Numerical examples

'Discontinuous' constant, linear and quadratic boundary elements were adopted for all analyses described below to avoid the difficulties which tend to occur in the vicinity of a 'corner'.

4.1 Square plasma

Assume hypothetical square plasma, 1.0m each side, as shown in **Fig.3**. The boundary condition $\psi = 0$ is imposed along each side of the square. In this case, an analytic solution exists **[3]** for the equation with a monomial $r^l z^m$ source term:

$$-\left\{ r\frac{\partial}{\partial r}\left(\frac{1}{r}\frac{\partial}{\partial r}\right)+\frac{\partial^2}{\partial z^2}\right\}\psi = r^l z^m \qquad (l \geq 0,\ m \geq 0)\ . \tag{72}$$

Fig.3 Square plasma

Section 4.1.1 Comparison between HBIE and SBIE solutions

Hyper singular boundary element analyses were performed using constant, discontinuous linear and discontinuous quadratic boundary elements for a monomial source $r^3 z^2$. In these three types of calculations, a total of 192 node points was commonly employed. That is, each side of the square was equally divided into 48, 24 and 16 boundary elements respectively for constant, linear and quadratic element computations.

As an evidence to show the validity of the present formulation, it was demonstrated that the values of the free term numerically given by Eq.(40) in **Section 2.6** were almost equal to the exact value,1/2. In the double precision computation with constant elements, for example, the values for 192 node points lie between 0.49999999269242 and 0.50000000496015.

Figure 4 shows the three types of HBIE results of $\partial\psi/\partial n$, the normal derivative of magnetic

flux along the boundary A-B-C-D-A shown in **Fig.3**. The analytic solution is also shown in **Fig.4**. The variation in $\partial\psi/\partial n$ is almost the same among the constant, the linear and the quadratic element HBIE computation results; large discrepancies are not found.

Fig.4 HBIE results of $\partial\psi/\partial n$ for r^3z^2 along the square boundary

The HBIE results were also compared with the SBIE esults. **Figure 5** represents only results obtained using constant boundary elements. In this comparison, discrepancies are found at points near the corners B and C; the HBIE results are a little larger than the SBIE results. The same tendencies were also found even when the linear and the quadratic elements were used.

Fig.5 Comparison between results of HBIE and SBIE calculations
using constant boundary elements for the square plasma

Figure 6(a) shows the contour map of magnetic flux, ψ, inside the domain, which was obtained through the HBIE analysis with discontinuous quadratic boundary elements. In contrast, **Fig.6(b)** shows the SBIE solution with the same boundary elements for the same problem. In both figures the solid lines denote the BEM solution, while the dashed lines show the analytic solution. Between the two BEM solutions of ψ shown in **Fig.6**, there does not seem to be much differences.

Fig.6 Contour maps of magnetic flux for the square plasma

However, the relative errors of the above quadratic element HBIE solution from the analytic one, defined by ε=((BEM-analytic)/analytic)$\times$100 %, are quite larger than those of the SBIE solution, as

shown in **Fig.7**. In **Table 1**, a total of 2500 internal points is categorized into four groups according to the different levels of the relative error. There is no point where the error is less than 0.1% in the hyper singular BIE calculation results. In contrast, in the standard BIE calculation results 2472 out of 2500 points, i.e., over 98.8% points represent less than 0.01% errors.

Fig.7 Relative errors in HBIE and SBIE solutions for the square plasma

Table 1 Error tendency in HBIE and SBIE solutions for the square plasma

Section 4.1.2 Refined mesh structures to improve the accuracy

Why are the large errors observed in the HBIE solutions in spite of the use of discontinuous boundary element? One possibility of the reason is that this square plasma geometry has the four 'corner' points. To improve the accuracy, the authors performed additional HBIE analyses with refined mesh structures of quadratic boundary elements applied in the vicinity of each corner point.

In the analyses, each side of the square was divided into one coarse mesh region (0.8m in length) and two fine mesh regions (0.1m long for each), as illustrated in **Fig.8**. On the coarse mesh region, 16 boundary elements were commonly used. In contrast, 10 (**Case 1**) or 20 (**Case 2**) boundary elements were employed on each fine mesh region. A total of 144 boundary elements (432 node points) was used for **Case 1**, while 224 boundary elements (672 node points) for **Case 2**.

Fig.8 Refined mesh structure for the square plasma problem

The relative errors in the HBIE solutions with these refined mesh structures were investigated. Contour maps of the error for Case 1 and Case 2 are respectively shown in **Fig.9(a)** and **Fig.9(b)**. The relative errors in both cases are also categorized into four groups in **Table 2**. Over 89.4% points

for Case 2 represent less than 0.01% errors. Apparently the accuracies in HBIE solutions have been improved by introducing the refined mesh structure, although the accuracies do not exceed the ones in SBIE solutions. It is suggested that one needs to employ a large number of node points in the vicinity of the corner to obtain accurate HBIE solutions for a geometry having corner points.

Fig.9 Relative errors in the refined SBIE solutions for the square plasma

Table 2 Error tendency in the refined HBIE solutions for the square plasma

One will investigate this effect of corner points again in the next section, dealing with a geometry that has no corner.

4.2 Circle plasma

One here considers circle plasma of radius 1.0m, center $(r, z) = (1.0m, 0.0m)$ in the $r - z$ plane. It should be noted that this circle boundary has no 'corner' points. One also assumes distributed source $\mu_0 r j_\varphi = r^3 z^2$ inside the circle, in the same way one performed for the square plasma in the previous section. For both HBIE and SBIE calculations, the circle boundary was equally divided into 60 discontinuous quadratic boundary elements so that 180 nodal points were located along the boundary.

The boundary condition $\psi = 0$ was imposed along the circle boundary. In this case, no analytic solution exists. Instead of a comparison with an analytic solution, one here investigates the relative deviation between the HBIE and SBIE solutions, which is defined by ε=((HBIE-SBIE)/SBIE)$\times$100%. As shown in **Fig.10** and **Table 3**, the relative deviations are quite small. Out of a total of 1900 internal points, 878 points (over 46.2%) show less than 0.001% deviations; 1806 points (over 95.0%) represent less than 0.01% deviations. This fact suggests that for a boundary having no corner point,

the accuracies of the HBIE solutions are almost the same as those in the SBIE calculations.

Fig.10 Relative deviation between HBIE and SBIE solutions for the circle plasma

Table 3 Tendency of deviation between HBIE and SBIE solutions for the circle plasma

4.3 Tokamak geometry

One here considers a problem of modelling the JT-60 tokamak-device. The reference solutions of plasma current density and magnetic flux had been obtained from an analysis using a reliable equilibrium code, SELENE, which is based on the finite element method **[14]**. An equilibrium computation was made based on a "hollow" current profile parametrization that has the form

$$\mu_0 r j_\varphi(r,\psi) = c_0\{\beta_p r^2 + (1-\beta_p)R_0^2\}(1+3X-4X^2)\,. \tag{73}$$

Here, $X=(\psi-\psi_M)/(\psi_S-\psi_M)$ in which ψ_M and ψ_S are the values of ψ on the magnetic axis and on the boundary, while β_p (= 0.70199) and R_0 (=3.39927 *m*) denote the poloidal beta and the characteristic major radius, respectively.

This problem was again analyzed using the hyper singular and the standard boundary element method. The boundary condition $\psi=0$ was imposed at each nodal point along the boundary. The same current profile parametrization shown above was again assumed. The complete polynomial of the 8-th order was adopted to approximate the $\mu_0 r j_\varphi$ distribution, and hence the polynomial consists of a total of 45 terms. To determine the polynomial expansion coefficients, a total of 1758 sampling points was automatically generated within the domain. The plasma boundary is approximated by a total of 57 discontinuous quadratic boundary elements, i.e., a total of 171 node points was employed.

As the source term given by Eq.(73) contains the unknowns of ψ, this problem must be solved as an eigenvalue problem **[3, 5, 15-17]**. A total of 7 iterations was required in the BEM analysis when

the relative eigenvalue deviation was reduced to less than 10^{-5}. The profiles of magnetic flux and current density thus obtained from the discontinuous quadratic BEM calculations are compared with the SELENE calculation results, as shown in **Fig.11** and **Fig.12**. In each figure, the solid lines show BEM solutions, while the dashed lines denote the reference results obtained using the SELENE code. Both HBIE and SBIE results show good agreement with the reference data.

Fig.11 Contour maps of HBIE results for JT-60

Fig.12 Contour maps of SBIE results for JT-60

Figure 13 shows maps of relative errors of magnetic flux results obtained through the HBIE and SBIE computations respectively compared with the SELENE reference solution, say, ε=((BIE-Reference)/Reference)$\times$100 %. The total of 1758 internal points is classified into three groups in **Table 4** according to the error levels. There is no large discrepancy of error tendency between the HBIE and the SBIE results, although near the boundary a larger number of points with more than 1.0% error are found in the HBIE results than in the SBIE results.

The 'X-point' indicated in **Fig.11(b)** and **Fig.12(b)** is only one 'corner' point in this tokamak problem. Why was the accuracy level in the HBIE solution almost the same as that in the SBIE solution in spite of the existence of X-point? One possible answer is that the accuracy in this case depends mainly on the polynomial approximation of current density distribution.

Fig.13 Relative errors in the BIE solutions of magnetic flux from the reference solution for JT-60

Table 4 Error tendency in HBIE and SBIE solutions for JT-60

5. Conclusions

This is the first work to solve the HBIE corresponding to the Grad-Shafranov equation. The HBIE has been regularized up to the level of the Cauchy principal value integral. All boundary integrals converge to finite values. Results of test calculations indicate the followings:

(1) The present approach to solve the HBIE provides stable and tolerably accurate numerical solutions.

(2) For a domain having corner points, the HBIE solutions are less accurate than the SBIE ones in spite of the use of discontinuous boundary elements. A finer mesh structure needs to be employed to improve the accuracy. Further effort must be made to investigate this reason.

(3) The discrepancy between the HBIE and the SBIE solutions is quite small for a circle domain that has no corner point.

(4) There is no large discrepancy between the HBIE and the SBIE solutions for the problem of actual fusion device, JT-60, where the current density distribution is approximated using a 2-D polynomial.

Acknowledgements

The authors wish to express their gratitude to Professor W.J. Mansur of COPPE / Federal University of Rio de Janeiro for his kind reply to their inquiry about the paper **[10]** dealing with a hyper singular boundary element formulation. Thanks are also due to Dr. K. Kurihara of Japan Atomic Energy Agency who kindly provided the authors with the reference tokamak plasma data used in the numerical demonstration in section 4.

References

[1] Wesson, J, "*Tokamaks (Second edition)*", The Oxford Engineering Series 48, Clarendon Press, Oxford (1997).

[2] Brebbia, C.A., "*The Boundary Element Method for Engineers*", Pentech Press, London (1978)

[3] Itagaki, M., Kamisawada, J., Oikawa, S., "Boundary- only integral equation approach based on polynomial expansion of plasma current profile to solve the Grad-Shafranov equation", *Nuclear Fusion*, **44**, 427-437 (2004).

[4] Itagaki, M., Yamaguchi, S., Fukunaga, T., "Boundary integral equation approach based on a polynomial expansion of the current distribution to reconstruct the current density profile in tokamak plasmas", *Nuclear Fusion*, **45**, 153-162 (2005).

[5] Itagaki, M., Fukunaga, T., "Boundary element modeling to solve the Grad-Shafranov equation as an axisymmetric problem", *Engineering Analysis with Boundary Elements*, **30**, 746-757 (2006).

[6] Krishnasamy, G., Rizzo, F.J., Rudolphi, T.J., "Hypersingular boundary integral equations: their occurrence, interpretation, regularization and computation", In: Banerjee, P.K., Kobayashi, S. (eds.) *Development in Boundary element Methods – Vol.7*, Elsevier applied Science, London and New York, 207-251 (1991).

[7] Guiggiani, M., Krishnasamy, M. Rudolphi, T.J., Rizzo, F.J., "A general algorithm for the numerical solution of hypersingular boundary integral equations", *ASME Journal of Applied Mechanics*", **59**, 604-614 (1992).

[8] Guiggiani, M., "Hypersingular boundary integral equations have an additional free term", *Computational Mechanics*, **16**, 245-248 (1995).

[9] Matsumoto, T., Tanaka, M., Hirata, H., “Boundary stress calculation using regularized boundary integral equation for displacement gradients”, *International Journal of Numerical Methods in Engineering*, **36**, 783-797 (1993).

[10] Mansur, W.J., Fleury Jr., P., Azevedo, J.P.S., “A vector approach to the hyper-singular BEM formulation for Laplace’s equation in 2D”, *International Journal of BEM Communications*, **8**, 239-250 (1997).

[11] Abramowitz, M., Stegun, I.A.: “*Handbook of Mathematical Functions*”, Dover Publications, New York (1965).

[12] Brebbia, C.A., Dominguez, J., “*Boundary Elements – An Introductory Course*”, Computational Mechanics Publications, Southampton (1992).

[13] Stroud, A.H., Secrest, D., “*Gaussian Quadrature Formulas*”, Prentice-Hall, New York (1966).

[14] Takeda, T., Tsunematsu, T., “*A Numerical Code SELENE To Calculate Axisymmetric Toroidal MHD Equilibria*”, JAERI-M 8042, Japan Atomic Energy Research Institute (1978).

[15] Watkins, D. S., “Fundamentals of Matrix Computations”, John Wiley & Sons, New York (1991).

[16] Mathews, J. H., Fink, K. D., “Numerical Methods Using MATLAB, Fourth Edition”, Pearson Prentice Hall, Upper Saddle River, New Jersey (2004).

[17] Itagaki, M., Sahashi, N., “Three-dimensional Multiple Reciprocity Boundary Element Method for Solving Neutron Diffusion Critical Eigenvalue Computations”, *J. Nucl. Sci. Tech.*, 33[2], 101-109 (1996)

Appendix List of derivatives of the fundamental solution for the Grad-Shafranov equation

The fundamental solution:

$$\psi^* = \frac{\sqrt{ar}}{\pi k}\left[\left(1-\frac{k^2}{2}\right)K(k)-E(k)\right] \tag{A1}$$

The derivatives:

$$\frac{\partial \psi^*}{\partial r} = \frac{r}{2\pi}\frac{1}{\sqrt{(r+a)^2+(z-b)^2}}\left[K(k)-\frac{r^2-a^2+(z-b)^2}{(r-a)^2+(z-b)^2}E(k)\right] \tag{A2}$$

$$\frac{\partial \psi^*}{\partial z} = -\frac{1}{2\pi}\frac{z-b}{\sqrt{(r+a)^2+(z-b)^2}}\left[-K(k)+\frac{r^2+a^2+(z-b)^2}{(r-a)^2+(z-b)^2}E(k)\right] \tag{A3}$$

$$\frac{\partial \psi^*}{\partial a} = \frac{a}{2\pi}\frac{1}{\sqrt{(r+a)^2+(z-b)^2}}\left[K(k)-\frac{a^2-r^2+(z-b)^2}{(r-a)^2+(z-b)^2}E(k)\right] \tag{A4}$$

$$\frac{\partial \psi^*}{\partial b} = -\frac{1}{2\pi}\frac{b-z}{\sqrt{(r+a)^2+(z-b)^2}}\left[-K(k)+\frac{r^2+a^2+(z-b)^2}{(r-a)^2+(z-b)^2}E(k)\right] \tag{A5}$$

$$\frac{\partial}{\partial a}\left(\frac{\partial \psi^*}{\partial r}\right) = -\frac{r+a}{(r+a)^2+(z-b)^2}\frac{\partial \psi^*}{\partial r}+\frac{r}{2\pi}\frac{1}{\sqrt{(r+a)^2(z-b)^2}}\frac{1}{(r-a)^2+(z-b)^2}$$

$$\times\left[\frac{r^2-a^2+(z-b)^2}{(r+a)^2+(z-b)^2}\left\{(r-a)K(k)+(r+a)E(k)\right\}-2rE(k)+\frac{4a(z-b)^2}{(r-a)^2+(z-b)^2}E(k)\right] \tag{A6}$$

$$\frac{\partial}{\partial b}\left(\frac{\partial \psi^*}{\partial r}\right) = \frac{z-b}{(r+a)^2+(z-b)^2}\frac{\partial \psi^*}{\partial r}+\frac{ar(z-b)}{\pi}\frac{1}{\sqrt{(r+a)^2+(z-b)^2}}\frac{1}{(r-a)^2+(z-b)^2}$$

$$\times\left[\frac{1}{(r+a)^2+(z-b)^2}\left\{(r-a)K(k)+(r+a)E(k)\right\}-\frac{2(r-a)}{(r-a)^2+(z-b)^2}E(k)\right] \tag{A7}$$

$$\frac{\partial}{\partial a}\left(\frac{\partial \psi^*}{\partial z}\right) = -\frac{r+a}{(r+a)^2+(z-b)^2}\frac{\partial \psi^*}{\partial z} + \frac{r(z-b)}{2\pi}\frac{1}{\sqrt{(r-a)^2+(z-b)^2}}\frac{1}{(r-a)^2+(z-b)^2}$$

$$\times\left[\frac{r^2-a^2+(z-b)^2}{(r+a)^2+(z-b)^2}\{K(k)+E(k)\} - 2E(k) - \frac{4a(r-a)}{(r-a)^2+(z-b)^2}E(k)\right] \quad \text{(A8)}$$

$$\frac{\partial}{\partial b}\left(\frac{\partial \psi^*}{\partial z}\right) = \left\{-\frac{1}{z-b} + \frac{z-b}{(r+a)^2+(z-b)^2}\right\}\frac{\partial \psi^*}{\partial z} + \frac{ar(z-b)^2}{\pi}\frac{1}{\sqrt{(r+a)^2+(z-b)^2}}\frac{1}{(r-a)^2+(z-b)^2}$$

$$\times\left[\frac{1}{(r+a)^2+(z-b)^2}\{K(k)+E(k)\} - \frac{2}{(r-a)^2+(z-b)^2}E(k)\right] \quad \text{(A9)}$$

List of Tables

Table 1 Error tendency in HBIE and SBIE solutions for the square plasma

Table 2 Error tendency in the refined HBIE solutions for the square plasma

Table 3 Tendency of deviation between HBIE and SBIE solutions for the circle plasma

Table 4 Error tendency in HBIE and SBIE solutions for JT-60

List of Figures

Fig.1 Boundary surface augmented by a small semicircle of radius ε

Fig.2 Quadratic boundary element

Fig.3 Square plasma

Fig.4 HBIE results of $\partial\psi/\partial n$ for r^3z^2 along the square boundary

Fig.5 Comparison between results of HBIE and SBIE calculations using constant boundary elements for the square plasma

Fig.6 Contour maps of magnetic flux for the square plasma

Fig.7 Relative errors in HBIE and SBIE solutions for the square plasma

Fig.8 Refined mesh structure for the square plasma problem

Fig.9 Relative errors in the refined SBIE solutions for the square plasma

Fig.10 Relative deviation between HBIE and SBIE solutions for the circle plasma

Fig.11 Contour maps of HBIE results for JT-60

Fig.12 Contour maps of SBIE results for JT-60

Fig.13 Relative errors in the BIE solutions of magnetic flux from the reference solution for JT-60

Table 1 Error tendency in HBIE and SBIE solutions for the square plasma

Range of error levels	HBIE	SBIE
$\varepsilon < 0.01\%$	0	2472
$0.01\% < \varepsilon < 0.1\%$	0	26
$0.1\% < \varepsilon < 1.0\%$	2258	2
$\varepsilon > 1.0\%$	242	0
Total	2500	2500

Table 2 Error tendency in the refined HBIE solutions for the square plasma

Range of error levels	Case 1 (144BEs)	Case 2 (224BEs)
$\varepsilon < 0.01\%$	1856	2236
$0.01\% < \varepsilon < 0.1\%$	594	260
$0.1\% < \varepsilon < 1.0\%$	50	4
$\varepsilon > 1.0\%$	0	0
Total	2500	2500

Table 3 Tendency of deviation between HBIE and SBIE solutions for the circle plasma

Range of deviation levels	Number of points
$\varepsilon < 0.001\%$	878
$0.001\% < \varepsilon < 0.01\%$	928
$\varepsilon > 0.01\%$	94
Total	1900

Table 4 Error tendency in HBIE and SBIE solutions for JT-60

Range of error levels	HBIE	SBIE
$\varepsilon < 0.1\%$	395	443
$0.1\% < \varepsilon < 1.0\%$	1294	1296
$\varepsilon > 1.0\%$	69	19
Total	1758	1758

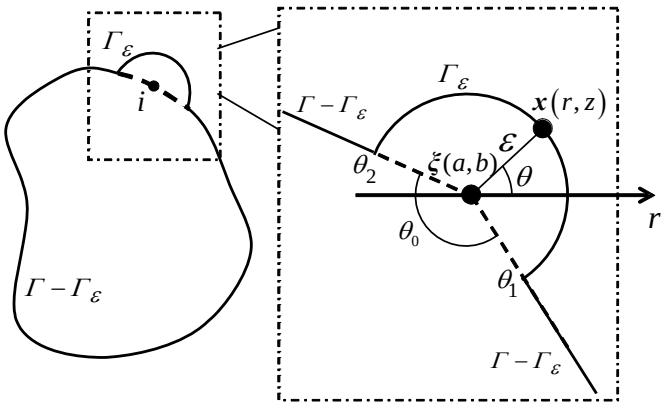


Fig.1 Boundary surface augmented by a small semicircle of radius ε

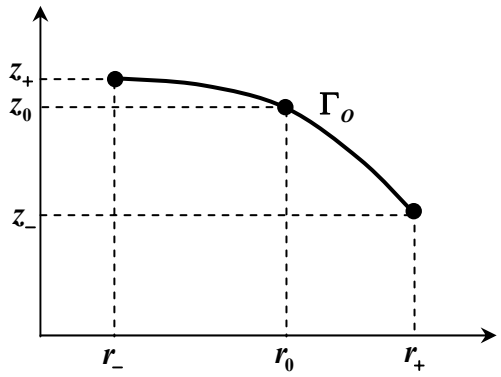


Fig.2 Quadratic boundary element

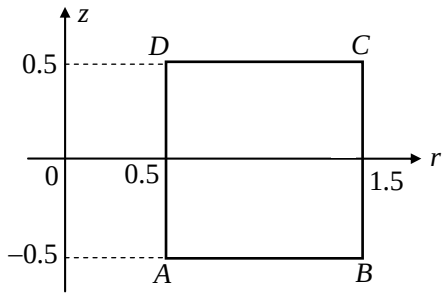


Fig.3 Square plasma

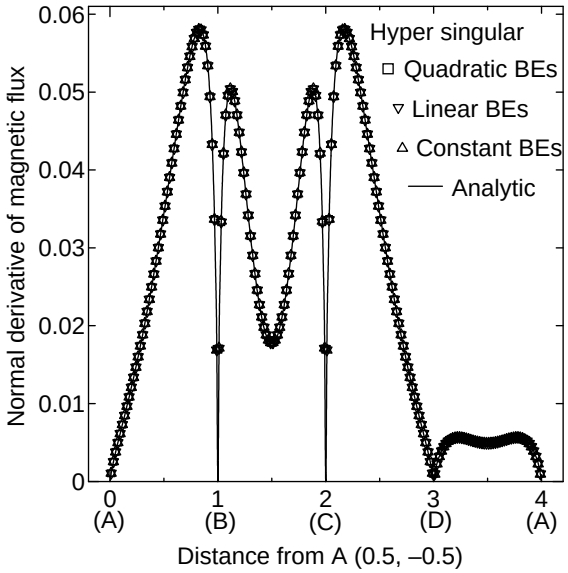


Fig.4 HBIE results of $\partial\psi/\partial n$ for r^3z^2 along the square boundary

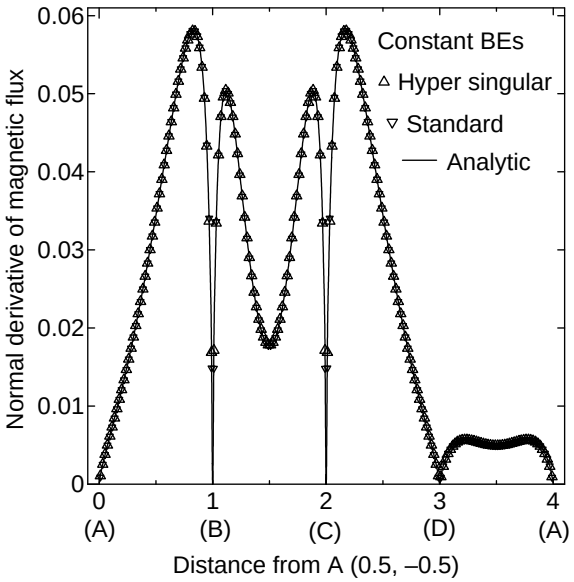
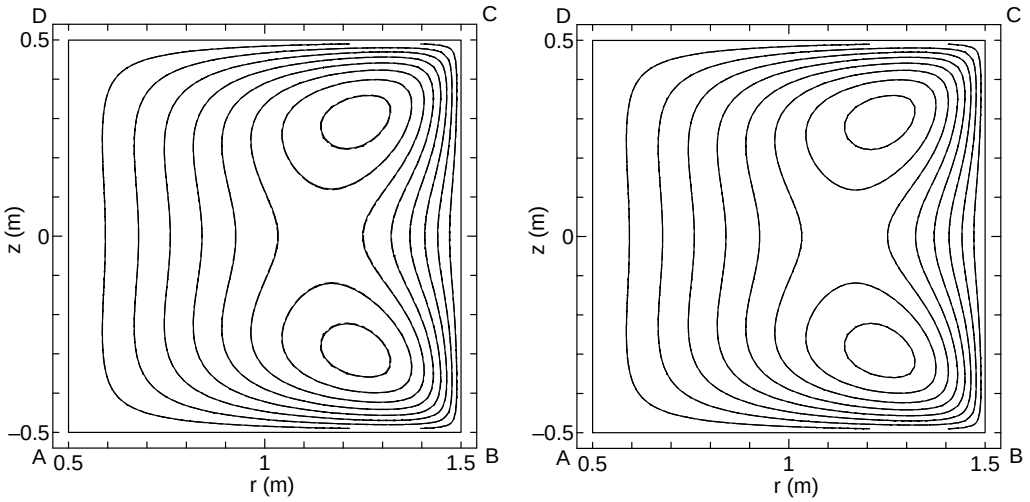
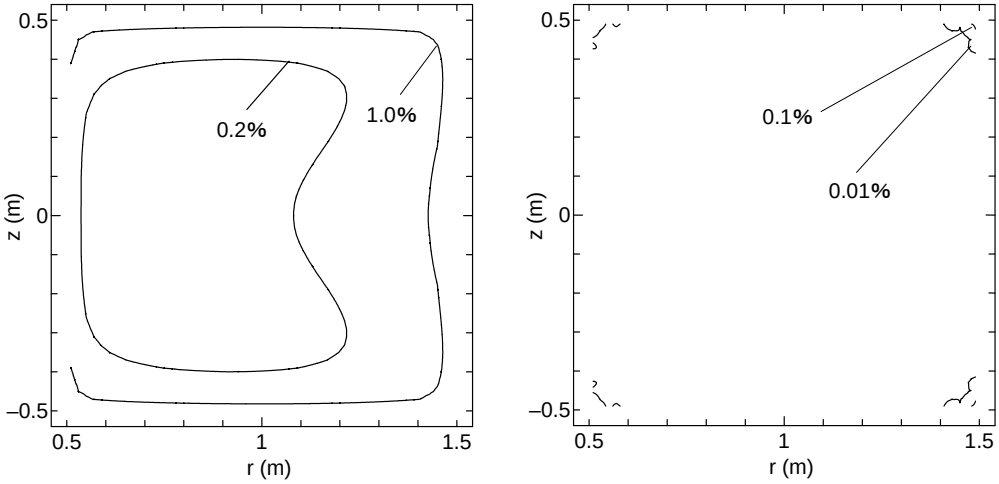


Fig.5 Comparison between results of HBIE and SBIE calculations using constant boundary elements for the square plasma



(a) HBIE solution (b) SBIE solution

Fig.6 Contour maps of magnetic flux for the square plasma



(a) HBIE (b) SBIE

Fig.7 Relative errors in HBIE and SBIE solutions for the square plasma

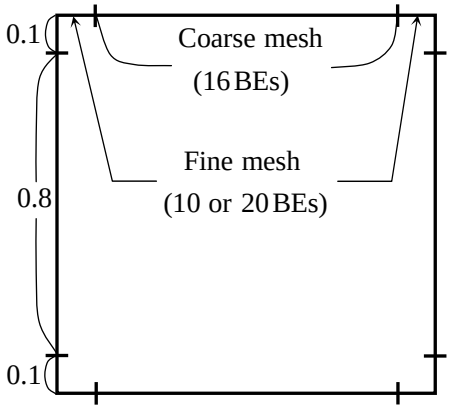
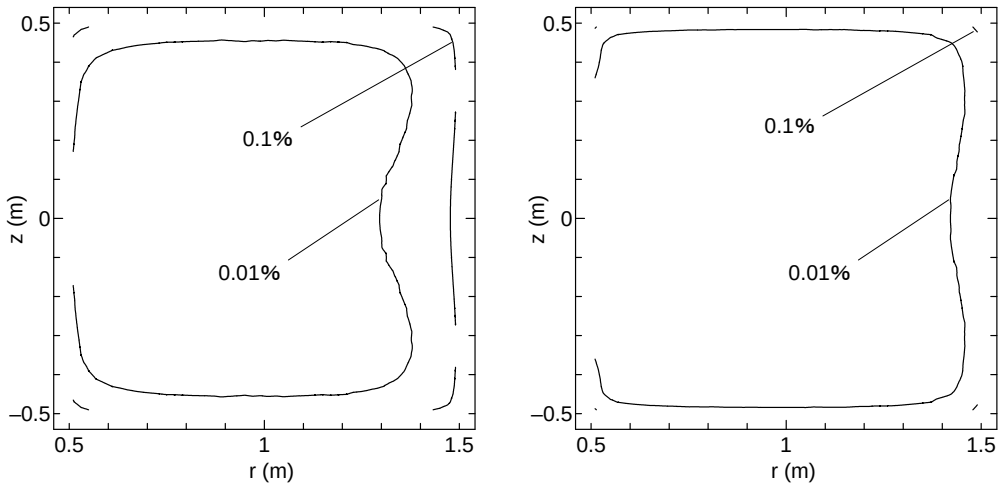


Fig.8 Refined mesh structure for the square plasma problem



(a) Case 1 (144BEs) (b) Case 2 (224BEs)

Fig.9 Relative errors in the refined SBIE solutions for the square plasma

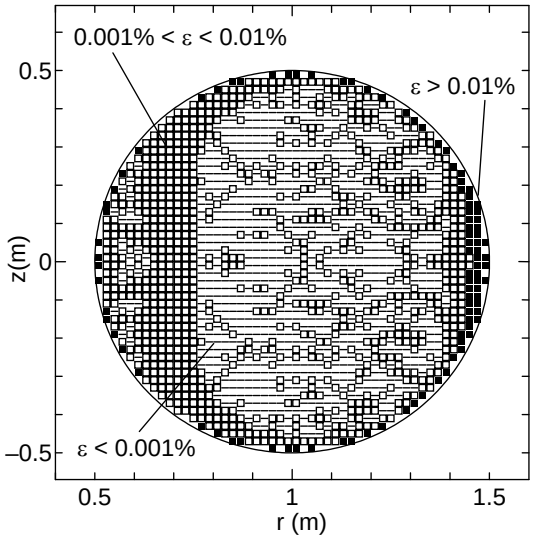
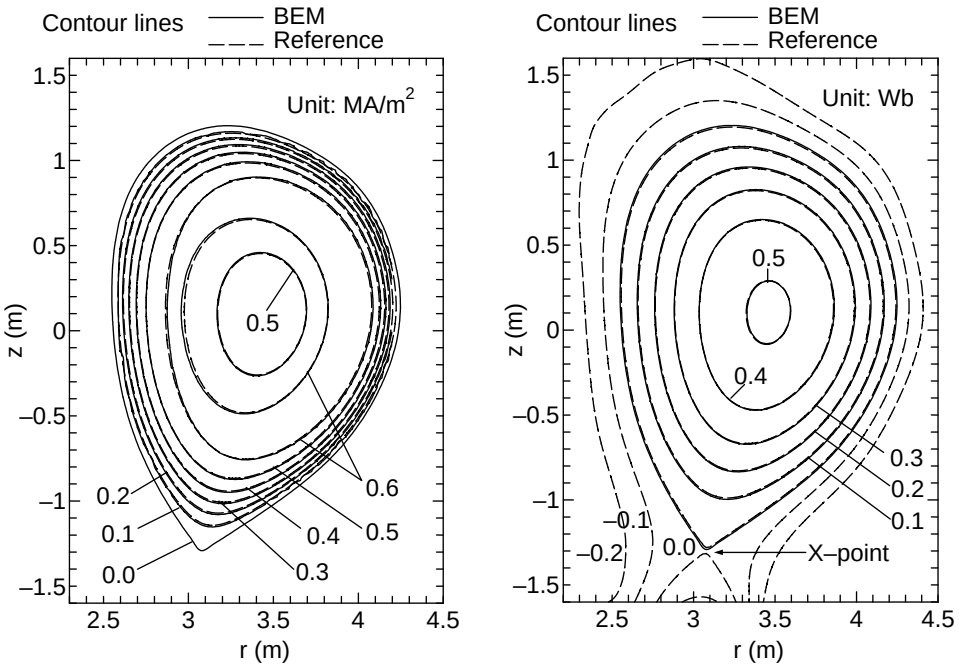
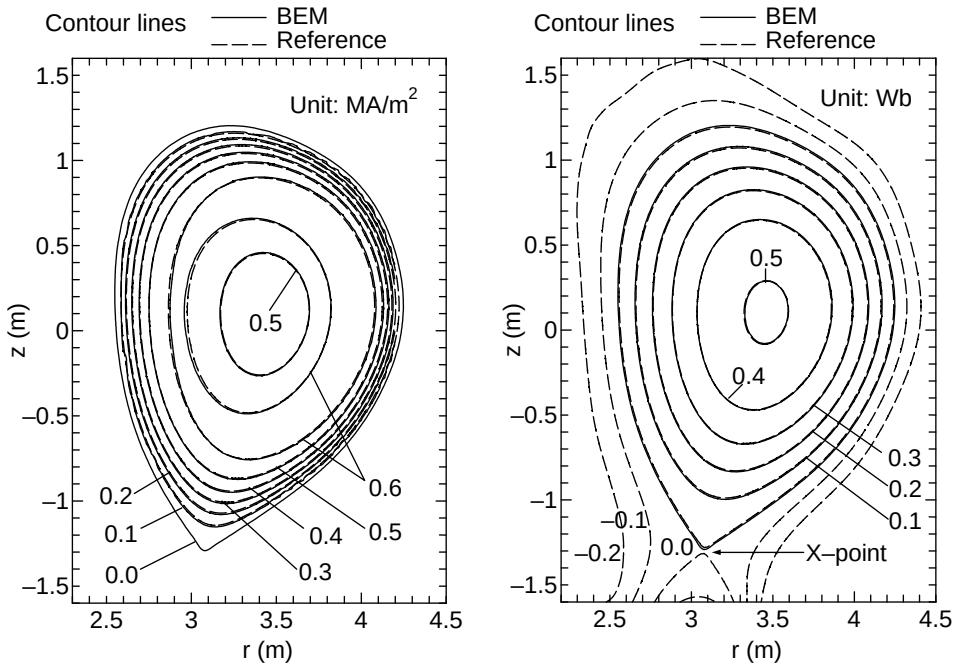


Fig.10 Relative deviation between HBIE and SBIE solutions for the circle plasma



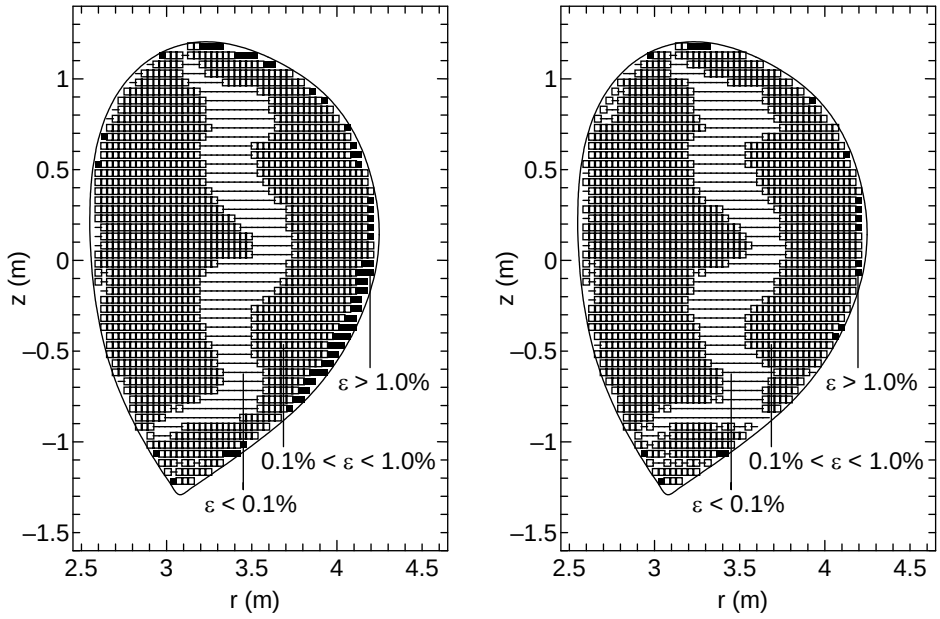
(a) Current density (b) magnetic flux

Fig.11 Contour maps of HBIE results for JT-60



(a) Current density (b) magnetic flux

Fig.12 Contour maps of SBIE results for JT-60



(a) Hyper singular (b) Standard

Fig.13 Relative errors in the BIE solutions of magnetic flux from the reference solution for JT-60